

# Exponentially accurate spectral and spectral element methods for fractional ODEs



Mohsen Zayernouri, George Em Karniadakis\*

Division of Applied Mathematics, Brown University, 182 George Street, Providence, RI 02912, USA

## ARTICLE INFO

### Article history:

Received 10 May 2013  
Received in revised form 5 September 2013  
Accepted 24 September 2013  
Available online 11 October 2013

### Keywords:

Jacobi polyfractonomials  
Petrov–Galerkin spectral methods  
Discontinuous spectral element method  
Exponential convergence

## ABSTRACT

Current discretizations of fractional differential equations lead to numerical solutions of low order of accuracy. Here, we present different methods for fractional ODEs that lead to exponentially fast decay of the error. First, we develop a Petrov–Galerkin (PG) spectral method for Fractional Initial-Value Problems (FIVPs) of the form  ${}_0\mathcal{D}_t^\nu u(t) = f(t)$  and Fractional Final-Value Problems (FFVPs)  ${}_t\mathcal{D}_t^\nu u(t) = g(t)$ , where  $\nu \in (0, 1)$ , subject to Dirichlet initial/final conditions. These schemes are developed based on a new spectral theory for fractional Sturm–Liouville problems (FSLPs), which has been recently developed in [1]. Specifically, we obtain solutions to FIVPs and FFVPs in terms of the new fractional (non-polynomial) basis functions, called *Jacobi polyfractonomials*, which are the eigenfunctions of the FSLP of *first* kind (FSLP-I). Correspondingly, we employ another space of test functions as the span of polyfractonomial eigenfunctions of the FSLP of *second* kind (FSLP-II). Subsequently, we develop a Discontinuous Spectral Method (DSM) of Petrov–Galerkin sense for the aforementioned FIVPs and FFVPs, where the basis functions do not satisfy the initial/final conditions. Finally, we extend the DSM scheme to a Discontinuous Spectral Element Method (DSEM) for efficient longer time-integration and adaptive refinement. In these discontinuous schemes, we employ the *asymptotic* eigensolutions to FSLP-I & -II, which are of Jacobi polynomial forms, as basis and test functions. Our numerical tests confirm the exponential/algebraic convergence, respectively, in  $p$ - and  $h$ -refinements, for various test cases with integer- and fractional-order solutions.

© 2013 Elsevier Inc. All rights reserved.

## 1. Introduction

Fractional differential operators of form  $\mathcal{D}_t^\nu \equiv d^\nu/dt^\nu$ , where  $\nu \in \mathbb{R}$ , appear in many systems in science and engineering such as electrochemical processes [2], porous or fractured media [3], viscoelastic materials [4,5], bioengineering applications [6]. For instance, it has been found that the transport dynamics in complex and/or disordered systems is governed by non-exponential relaxation patterns and *anomalous* diffusion [7–9]. For such non-Markovian processes, a time-fractional diffusion equation, in which the time-derivative emerges as  $\mathcal{D}_t^\nu u(t)$ , governs the evolution for the Probability Density Function (PDF). Another interesting example occurring in viscous fluid flows is the *cumulative memory* effect of the wall-friction through the boundary layer, which gives rise to fractional derivatives in equations of fluid motion [10–12].

Over the last two decades, the notion of fractional derivative has been extended to many ordinary fractional differential equations (FODEs) such as fractional Cauchy equation, fractional Gauss equations [13,14] and fractional Sturm–Liouville equation [15], in addition to a variety of fractional partial differential equations (FPDEs) such as fractional Fokker–Planck equation [16], fractional Burgers' equation [17], and fractional advection–diffusion equation [18]. In these problems, the

\* Corresponding author. Fax: +1 (401) 863 2722.

E-mail address: [george\\_karniadakis@brown.edu](mailto:george_karniadakis@brown.edu) (G.E. Karniadakis).

corresponding differential operators can be defined based on different but closely related ways. The extension of existing numerical methods for integer-order differential equations ([19–23] and references therein) to their corresponding fractional differential equations (FDEs) is not trivial. While the approximation of these models is computationally demanding due to their long-range *history*-dependence, the development of numerical schemes in this area does not have a long history, and has undergone a fast evolution. Depending on how (temporal  $\mathcal{D}_t^\nu$  or spatial  $\mathcal{D}_x^\nu$ ) fractional derivatives are discretized and according to their order of accuracy, different classes of numerical methods have been developed in the literature.

### 1.1. Finite difference methods (FDM)

To our knowledge, Lubich [24,25] is the pioneer of the idea of *discretized fractional calculus* within the spirit of finite difference method (FDM). Later, Sanz-Serna [26] adopted the idea of Lubich and presented a temporal semi-discrete algorithm for partial integro-differential equations, which was first order accurate. Sugimoto [17] also employed an FDM for approximating the fractional derivative emerging in Burgers' equation. Later on, the paper of Metzler and Klafter [8] opened a new horizon toward FPDEs by introducing a fractional dynamics approach to time-fractional diffusion. Subsequently, Gorenflo et al. [27] adopted a finite difference scheme by which they could generate discrete models of random walk in such anomalous diffusion. Diethelm et al. proposed a predictor–corrector scheme in addition to a fractional Adams method [13, 28]. After that, Langlands and Henry [29] considered the fractional diffusion equation, and analyzed the  $L^1$  scheme for the time-fractional derivative. Sun and Wu [30] also constructed a difference scheme with  $L^\infty$  approximation of time-fractional derivative. In order to develop and analyze higher-order FDM schemes Lin and Xu [31] analyzed an FDM for the discretization of the time-fractional diffusion equation with order  $(2 - \alpha)$ . Kumar and Agrawal [32] proposed a block-by-block method for a class of fractional initial-value problems which later Huang et al. [33] proved that it enjoys a rate of convergence of at least 3. Recently, Cao and Xu [34] rigorously developed the scheme to  $(3 + \alpha)$ -th order,  $\alpha \in (0, 1)$ . To the best of knowledge, this is the highest-order and the most recent FDM scheme for discretization of fractional derivatives.

Although implementation of such FDM approaches is relatively easy, their biggest issue is that the accuracy is limited. Moreover, these approaches suffer from heavy cost of computing the long-ranged memory in discretization of the fractional derivatives at each point. In fact, FDM is inherently a *local* approach whereas fractional derivatives are essentially *global* (nonlocal) differential operators. This property would suggest that global schemes such as *Spectral Methods* (SMs) are more appropriate tools for discretizing fractional differential equations.

### 1.2. Spectral methods (SMs)

Unlike the attention put on developing FDM schemes, very little effort has been put on developing rigorous high-order spectral methods. A Fourier SM was utilized by Sugimoto [17] in a fractional Burgers' equation, linearized by Taylor expansion, and a spline-based collocation method was employed by Blank [35] for numerical treatment of a class of FODEs. This approach was later employed by Rawashdeh [36] for solving fractional integro-differential equations. In these works, the expected high convergence rate was not observed and no error/stability analysis was carried out. Lin and Xu [31] developed a hybrid scheme for time-fractional diffusion problem, treating the time-fractional derivative using FDM and discretizing the *integer-order* spatial derivative by a Legendre SM. In such mixed approaches, the error associated with the low-order temporal accuracy can easily dominate the global error, for instance when the time-dependent portion of the exact solution is discontinuous, or if is a monomial of form  $t^n$ , where  $n$  is sufficiently large, or is a smooth function e.g.,  $\sin(n\pi t)$ . The idea of collocation was later adopted by Khader [37], where he proposed a Chebyshev collocation method for the discretization of the space-fractional diffusion equation. More recently, Khader and Hendy [38] developed a Legendre pseudospectral method for fractional-order delay differential equations.

The collocation and pseudospectral schemes for fractional equations are relatively easy to implement but their performance has not been tested thoroughly. For instance, when the exact solution is of polynomial form it is claimed that a fast convergence is observed. However, for other test cases no such exponential-like convergence is achieved. The first fundamental work on spectral methods for FPDEs was done by Li and Xu [39,40] who developed a space–time SM for time-fractional diffusion equation. To the best of our knowledge, they were the first who achieved *exponential* convergence in their numerical tests in agreement with their error analysis. However, in this scheme, the corresponding stiffness and mass matrices are dense and gradually become ill-conditioned when the fractional order  $\alpha$  tends to small values. Moreover, this approach is not effective e.g., when the forcing term exhibits discontinuity in the time-domain. This, in turn, motivates the use of domain decomposition and *Finite Element Methods* (FEM) and *Spectral Element Methods* (SEM) in the context of fractional calculus.

### 1.3. Spectral/hp element methods

A theoretical framework for the least-square finite element approximation of a fractional-order differential equation was developed by Fix and Roop [41], where optimal error estimates are proven for piecewise linear trial elements. The main hurdle to overcome in FEM is the nonlocal nature of the fractional operator which leads to large dense matrices; even construction of such matrices presents difficulties [42]. There are, however, a number of recent works already employed in this area using FEM to obtain more efficient schemes. McLean and Mustapha [43] developed a piecewise-constant discontinuous

Galerkin method for the time discretization of a sub-diffusion equation. Hanert [44] also considered the use of a Chebyshev spectral element method for the numerical solution of the fractional-order transport. Recently, the idea of the least-square FEM [41] was extended to the spectral element method by Carella [45]. Despite the spectral expansion, these schemes are not properly formulated and fail to achieve exponential convergence.

In this paper, we develop exponentially accurate numerical schemes of Petrov–Galerkin type for the FODEs of form  ${}_0\mathcal{D}_t^\nu u(t) = f(t)$  and  ${}_t\mathcal{D}_T^\nu u(t) = f(t)$ , introduced, respectively, as Fractional Initial-Value Problem (FIVP) and Fractional Final-Value Problem (FFVP) subject to Dirichlet initial/final conditions. To this end, we first develop a Petrov–Galerkin (PG) spectral method whose corresponding stiffness matrix is *diagonal*. Subsequently, we develop a Discontinuous Spectral Method (DSM) of Petrov–Galerkin sense with *exact* quadrature rules for the aforementioned FIVPs and FFVPs. This scheme is also extended to a discontinuous spectral element method (DSEM) for efficient longer time-integrations and adaptive refinement. These schemes are developed based on a new spectral theory for fractional Sturm–Liouville problems (FSLPs), which has been recently developed in [1]. In order to test the performance of our schemes,  $p$ -refinement and  $h$ -refinement tests are performed for a range of test cases, where the exact solution is a monomial  $t^n$ ,  $n \in \mathbb{N}$ , fractonomial  $t^{n+\mu}$ ,  $\mu \in (0, 1)$ , (see [1]), smooth functions of form  $t^p \sin(n\pi t)$ ,  $p \in \mathbb{N}$ , fractional functions  $t^{n_1+\mu_1} \sin(n\pi t^{n_2+\mu_2})$ ,  $n_1, n_2 \in \mathbb{N}$  and  $\mu_1, \mu_2 \in (0, 1)$ , or any combinations of these functions.

**2. Notation and definitions**

We first introduce the simplest fractional ordinary differential equation (FODE), which forms a building block for the construction of other fractional differential operators. Here, we define the Fractional Initial-Value Problem (FIVP) of order  $\nu \in (0, 1)$  as

$$\begin{aligned} {}_0\mathcal{D}_t^\nu u(t) &= f(t), \quad t \in (0, T], \\ u(0) &= u_0, \end{aligned} \tag{1}$$

where  ${}_0\mathcal{D}_t^\nu$  denotes the left-sided Riemann–Liouville fractional derivative of order  $\nu \in (0, 1)$  following [46], defined as

$${}_0\mathcal{D}_t^\nu u(t) = \frac{1}{\Gamma(1-\nu)} \frac{d}{dt} \int_0^t \frac{u(s) ds}{(t-s)^\nu}, \quad t > 0, \tag{2}$$

where  $\Gamma$  represents the Euler gamma function.

Next, we define the corresponding Fractional Final-Value Problem (FFVP) of order  $\nu \in (0, 1)$ , for which the final value of the unknown solution is given as

$$\begin{aligned} {}_t\mathcal{D}_T^\nu u(t) &= g(t), \quad t \in [0, T), \\ u(T) &= u_T, \end{aligned} \tag{3}$$

where  ${}_t\mathcal{D}_T^\nu$  represents the right-sided Riemann–Liouville fractional derivative of order  $\nu \in (0, 1)$ , defined as

$${}_t\mathcal{D}_T^\nu u(t) = \frac{1}{\Gamma(1-\nu)} \left( \frac{-d}{dt} \right) \int_t^T \frac{u(s) ds}{(s-t)^\nu}, \quad t < T. \tag{4}$$

We also define the fractional differential operators in (1) and (3) to be the Caputo fractional derivatives  ${}_0^C\mathcal{D}_t^\nu$  and  ${}_t^C\mathcal{D}_T^\nu$ , respectively. In fact, these fractional operators can be defined by (2) and (4), in which the order of the integration and first derivative is reversed. However, the two definitions are linked by the following relationships

$${}_0\mathcal{D}_t^\nu u(t) = \frac{u(0)}{\Gamma(1-\nu)t^\nu} + {}_0^C\mathcal{D}_t^\nu u(t), \tag{5}$$

and

$${}_t\mathcal{D}_T^\nu u(t) = \frac{u(T)}{\Gamma(1-\nu)(T-t)^\nu} + {}_t^C\mathcal{D}_T^\nu u(t). \tag{6}$$

Hence, when  $u_0 = 0$  and  $u_T = 0$  in (1) and (3), these problems become identical to the corresponding problems with the Caputo derivatives by virtue of (5) and (6).

**3. Petrov–Galerkin (PG) spectral method**

First, we develop a spectral method for the FIVP (1), subject to homogeneous Dirichlet initial conditions. Then, we generalize the scheme for non-zero Dirichlet initial conditions.

### 3.1. Basis functions

Our spectral scheme is based upon a new spectral theory for fractional Sturm–Liouville eigen-problems (FSLP), developed in [1]. Accordingly, we seek the solution to the FIVPs in terms of the new fractional (non-polynomial) basis functions, called *Jacobi polyfractonomials*, which are the eigenfunctions of the FSLP of first kind, explicitly obtained as

$${}^{(1)}\mathcal{P}_n^{\alpha,\beta,\mu}(x) = (1+x)^{-\beta+\mu-1} P_{n-1}^{\alpha-\mu+1,-\beta+\mu-1}(x), \quad x \in [-1, 1], \tag{7}$$

where  $P_{n-1}^{\alpha-\mu+1,-\beta+\mu-1}(x)$  are the standard Jacobi polynomials in which  $\mu \in (0, 1)$ ,  $-1 \leq \alpha < 2 - \mu$ , and  $-1 \leq \beta < \mu - 1$ . Particularly,  ${}^{(1)}\mathcal{P}_n^{\alpha,\beta,\mu}(x)$  represent the eigenfunctions of the *singular* FSLP of first kind (SFSLP-I) when  $\alpha \neq -1$  and  $\beta \neq -1$ ; otherwise  ${}^{(1)}\mathcal{P}_n^\mu(x) \equiv {}^{(1)}\mathcal{P}_n^{-1,-1,\mu}(x)$  denote the eigenfunctions of the *regular* FSLP of first kind (RFSLP-I). Moreover, it has been shown in [1] that both sets of regular  $\{{}^{(1)}\mathcal{P}_n^\mu(x)\}_{n=1}^N$  and singular bases  $\{{}^{(1)}\mathcal{P}_n^{\alpha,\beta,\mu}(x)\}_{n=1}^N$  (for some  $N \in \mathbb{N}$ ) have identical approximating properties when  $\alpha = \beta$ . Hence, in this work and for simplicity, we employ the fractional eigenfunctions for  $\alpha = \beta = -1$ :

$${}^{(1)}\mathcal{P}_n^\mu(x) = (1+x)^\mu P_{n-1}^{-\mu,\mu}(x), \quad x \in [-1, 1], \tag{8}$$

as our basis functions. Now, let  $u_0 = 0$  and  $t \in [0, T]$ . Then,

$${}^{(1)}\tilde{\mathcal{P}}_n^\mu(t) = \left(\frac{2}{T}\right)^\mu t^\mu P_{n-1}^{-\mu,\mu}(x(t)) \tag{9}$$

represent the shifted basis functions of fractional order  $(n - 1 + \mu)$  that is obtained through the affine mapping  $x = 2t/T - 1$ , transforming the standard interval  $[-1, 1]$  to  $[0, T]$ . From the properties of the eigensolutions in [1], the left-sided Riemann–Liouville fractional derivative of (9) is given as

$${}_0\mathcal{D}_t^\mu ({}^{(1)}\tilde{\mathcal{P}}_n^\mu(x(t))) = \left(\frac{2}{T}\right)^\mu {}_{-1}\mathcal{D}_x^\mu ({}^{(1)}\mathcal{P}_n^\mu(x)) = \left(\frac{2}{T}\right)^\mu \frac{\Gamma(n+\mu)}{\Gamma(n)} P_{n-1}(x(t)), \tag{10}$$

stating that the  $\mu$ -th order fractional derivative of such fractional (non-polynomial) basis functions of order  $(n - 1 + \mu)$  is a standard Legendre polynomials of integer order  $(n - 1)$ . Moreover, since  $u(0) = u_0 = 0$ , the aforementioned Riemann–Liouville fractional derivative is identical to the one of Caputo type by virtue of (5).

### 3.2. Test functions

In order to obtain the variational form in the Petrov–Galerkin spectral method, we test (1) against a different set of test functions, which are in fact the eigenfunctions of the FSLP of second kind, explicitly obtained in [1] as

$${}^{(2)}\mathcal{P}_k^{\alpha,\beta,\mu}(x) = (1-x)^{-\alpha+\mu-1} P_{k-1}^{-\alpha+\mu-1,\beta-\mu+1}(x), \quad x \in [-1, 1], \tag{11}$$

which belong to another family of the Jacobi polyfractonomials, where this time  $-1 \leq \alpha < 1 - \mu$ , and  $-1 \leq \beta < 2\mu - 1$ . By the same argument made in Section 3.1, we employ the following fractional test functions

$${}^{(2)}\mathcal{P}_k^\mu(x) = (1-x)^\mu P_{k-1}^{\mu,-\mu}(x), \quad x \in [-1, 1], \tag{12}$$

in our weak formulation. By carrying out the same affine mapping  $x = 2t/T - 1$ , we can obtain the shifted test functions

$${}^{(2)}\tilde{\mathcal{P}}_k^\mu(x(t)) = \left(\frac{2}{T}\right)^\mu (T-t)^\mu P_{k-1}^{\mu,-\mu}(x(t)), \tag{13}$$

corresponding to the interval  $[0, T]$ . Now, following [1], the right-sided Riemann–Liouville fractional derivative of (13) is obtained as

$${}_t\mathcal{D}_T^\mu ({}^{(2)}\tilde{\mathcal{P}}_k^\mu(t)) = \left(\frac{2}{T}\right)^\mu {}_x\mathcal{D}_{+1}^\mu ({}^{(2)}\mathcal{P}_k^\mu(x)) = \left(\frac{2}{T}\right)^\mu \frac{\Gamma(k+\mu)}{\Gamma(k)} P_{k-1}(x(t)) = {}_0\mathcal{D}_t^\mu ({}^{(1)}\tilde{\mathcal{P}}_k^\mu(t)), \tag{14}$$

where the last equality holds by (10). The relations in (14) also hold for the Caputo fractional derivatives thanks to (6).

Having defined the basis and test functions, next we will present the Petrov–Galerkin spectral method by recalling the following lemma.

**Lemma 3.1.** (See [39].) For all  $0 < \xi < 1$ , if  $u \in H^1([0, T])$  and  $w \in H^{\xi/2}([0, T])$ , then

$$({}_0\mathcal{D}_t^\xi u, w)_{[0,T]} = ({}_0\mathcal{D}_t^{\xi/2} u, {}_t\mathcal{D}_T^{\xi/2} w)_{[0,T]}, \tag{15}$$

where  $(\cdot, \cdot)_{[0,T]}$  denotes the standard inner product in the interval  $[0, T]$ .

3.3. PG spectral method for the FIVP

In FIVP (1), we seek an approximate solution of the form

$$u(t) \approx u_N(t) = \sum_{n=1}^N a_n {}^{(1)}\tilde{\mathcal{P}}_n^\mu(t), \tag{16}$$

where  $a_n$  are the unknown expansion coefficients to be determined. By plugging (16) into (1), we obtain the residual  $R_N(t)$  as

$$R_N(t) = {}_0\mathcal{D}_t^\nu u_N(t) - f(t)$$

to be  $L^2$ -orthogonal to all elements in the set of test functions  $\{{}^{(2)}\tilde{\mathcal{P}}_k^\mu(x(t)): k = 1, 2, \dots, N\}$  as

$$\sum_{n=1}^N a_n \int_0^T {}_0\mathcal{D}_t^{\nu(1)} \tilde{\mathcal{P}}_n^\mu(t) {}^{(2)}\tilde{\mathcal{P}}_k^\mu(x(t)) dt = \int_0^T f(t) {}^{(2)}\tilde{\mathcal{P}}_k^\mu(x(t)) dt.$$

Now, we choose  $\mu = \nu/2$ , and by Lemma 3.1, we obtain

$$\sum_{n=1}^N a_n \int_0^T {}_0\mathcal{D}_t^{\mu(1)} \tilde{\mathcal{P}}_n^\mu(t) {}_t\mathcal{D}_T^{\mu(2)} \tilde{\mathcal{P}}_k^\mu(x(t)) dt = \int_0^T f(t) {}^{(2)}\tilde{\mathcal{P}}_k^\mu(x(t)) dt,$$

where by (10) and (14) we obtain

$$\begin{aligned} \sum_{n=1}^N a_n \left(\frac{2}{T}\right)^{2\mu} \binom{n+\mu}{n} \binom{k+\mu}{k} \int_0^T P_{n-1}(x(t)) P_{k-1}(x(t)) dt &= \sum_{n=1}^N a_n \left(\frac{2}{T}\right)^{2\mu-1} \binom{n+\mu}{n}^2 \frac{2}{2n-1} \delta_{nk} \\ &= \int_0^T f(t) {}^{(2)}\tilde{\mathcal{P}}_k^\mu(x(t)) dt, \end{aligned}$$

which yields a diagonal stiffness matrix on the left-hand side, whose diagonal entries are given by  $\gamma_k = \left(\frac{2}{T}\right)^{2\mu-1} \left(\frac{k+\mu}{k}\right)^2 \frac{2}{2k-1}$ . Consequently, we obtain the expansion coefficients as

$$a_k = \frac{1}{\gamma_k} \int_0^T f(t) {}^{(2)}\tilde{\mathcal{P}}_k^\mu(x(t)) dt. \tag{17}$$

For the case of non-homogeneous initial conditions when  $u(0) = u_0 \neq 0$ , we employ the method of *lifting a known solution*, where we decompose the solution  $u(t)$  into two parts as

$$u(t) = u_{\mathcal{H}}(t) + u_{\mathcal{D}}, \tag{18}$$

in which  $u_{\mathcal{H}}(t)$  corresponds to the homogeneous solution and  $u_{\mathcal{D}} \equiv u_0$  is the non-zero initial condition, given in (1). We substitute (18) into (1) and take the fractional derivative on the known  $u_{\mathcal{D}}$  to the right-hand side to obtain

$$\begin{aligned} {}_0\mathcal{D}_t^\nu u_{\mathcal{H}}(t) &= h(t), \quad t \in (0, T], \\ u_{\mathcal{H}}(0) &= 0, \end{aligned} \tag{19}$$

where  $h(t) = f(t) - \frac{u_{\mathcal{D}}}{\Gamma(1-\nu)t^\nu}$ . We note that if we replace the fractional derivative in (19) by a Caputo one, the same scheme can be used, where this time  $h(t) \equiv f(t)$ , since the Caputo fractional derivative of the constant initial value  $u_0 (= u_{\mathcal{D}})$  is identically zero.

In Fig. 1, we present numerical results obtained using the PG spectral method to solve the fractional initial-value problem  ${}_0\mathcal{D}_t^\nu u(t) = f(t)$ ,  $t \in [0, 1]$ , corresponding to  $\nu = 1/10$  and  $9/10$ . Here we consider four different exact solutions: (i) monomial  $u^{ext}(t) = t^{10}$ , (ii) smooth function  $u^{ext}(t) = t^6 \sin(\pi t)$ , (iii) fractional function  $u^{ext}(t) = t^{13/2} \sin(\pi t^{4/3})$ , and finally (iv) combination of fractonomials (see [1]) and a smooth function  $u^{ext}(t) = t^6 \exp(t^2) + t^{8+5/7} + t^{10+1/3}$ . In all aforementioned cases exponential convergence is observed.

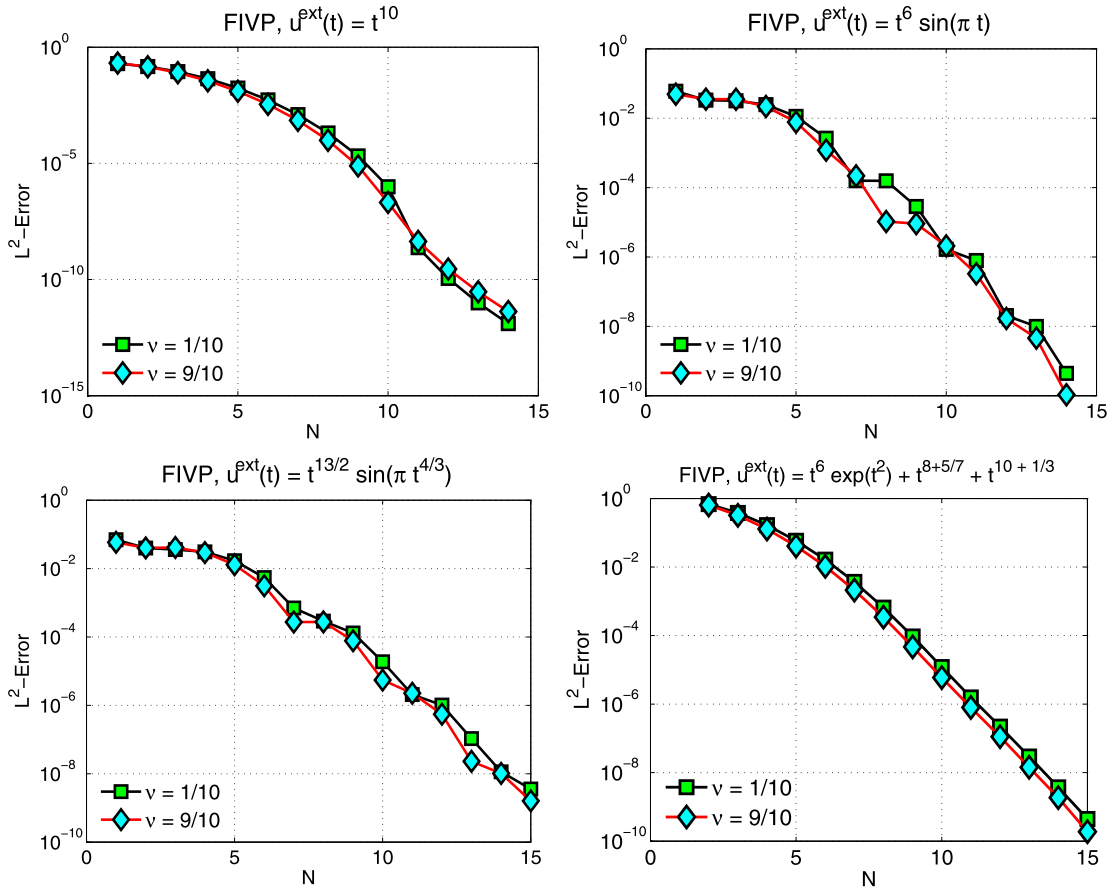


**Fig. 1.** PG spectral method for FIVP: log-linear  $L^2$ -error of the numerical solution to  ${}_0\mathcal{D}_t^\nu u(t) = f(t)$ ,  $t \in [0, 1]$ , versus  $N$ , the order-index in (16), corresponding to  $\nu = 1/10$  and  $9/10$ : (top-left) the exact solution  $u^{\text{ext}}(t) = t^{10}$ , (top-right)  $u^{\text{ext}}(t) = t^6 \sin(\pi t)$ , (bottom-left)  $u^{\text{ext}}(t) = t^{13/2} \sin(\pi t^{4/3})$ , and (bottom-right)  $u^{\text{ext}}(t) = t^6 \exp(t^2) + t^{8+5/7} + t^{10+1/3}$ .

3.4. PG spectral method for the FFVP

The numerical scheme for the FFVP (3) is similar to the one we developed in Section 3.3, except that we interchange the space of basis and test functions in the new scheme. In fact, we choose  $\{^{(2)}\tilde{\mathcal{P}}_j^\mu(t) : j = 1, 2, \dots, N\}$  to be set of basis functions, and we consider  $\{^{(1)}\tilde{\mathcal{P}}_k^\mu(t) : k = 1, 2, \dots, N\}$  as the set of test functions in deriving the variational form. Here, we seek the approximate solution to (3) of form

$$u(t) \approx u_N(t) = \sum_{j=1}^N b_j {}^{(2)}\tilde{\mathcal{P}}_j^\mu(t), \tag{20}$$

where  $b_j$  are the unknown expansion coefficients. By plugging (20) into (3) and requiring the corresponding residual function  $R_N(t)$  to be  $L^2$ -orthogonal to each element in the set of the test functions, we obtain the unknown coefficients as

$$b_k = \frac{1}{\gamma_k} \int_0^T f(t) {}^{(1)}\tilde{\mathcal{P}}_k^\mu(x(t)) dt. \tag{21}$$

When  $u(T) = u_T \neq 0$ , we employ again the method of lifting a known solution. We then decompose  $u(t)$  as shown in (18) and substitute it into (3) to obtain the following equivalent finite-value problem

$$\begin{aligned} {}_t\mathcal{D}_T^\nu u_{\mathcal{H}}(t) &= w(t), \quad t \in [0, T), \\ u_{\mathcal{H}}(T) &= 0, \end{aligned} \tag{22}$$

where  $w(t) = f(t) - \frac{u_T}{T(1-\nu)(T-t)^\nu}$ . In Fig. 2, we present numerical results obtained by the PG spectral method to solve the fractional final-value problem  ${}_t\mathcal{D}_T^\nu u(t) = f(t)$ ,  $t \in [0, 1]$ , corresponding to  $\nu = 1/10$  and  $9/10$ . We consider four different

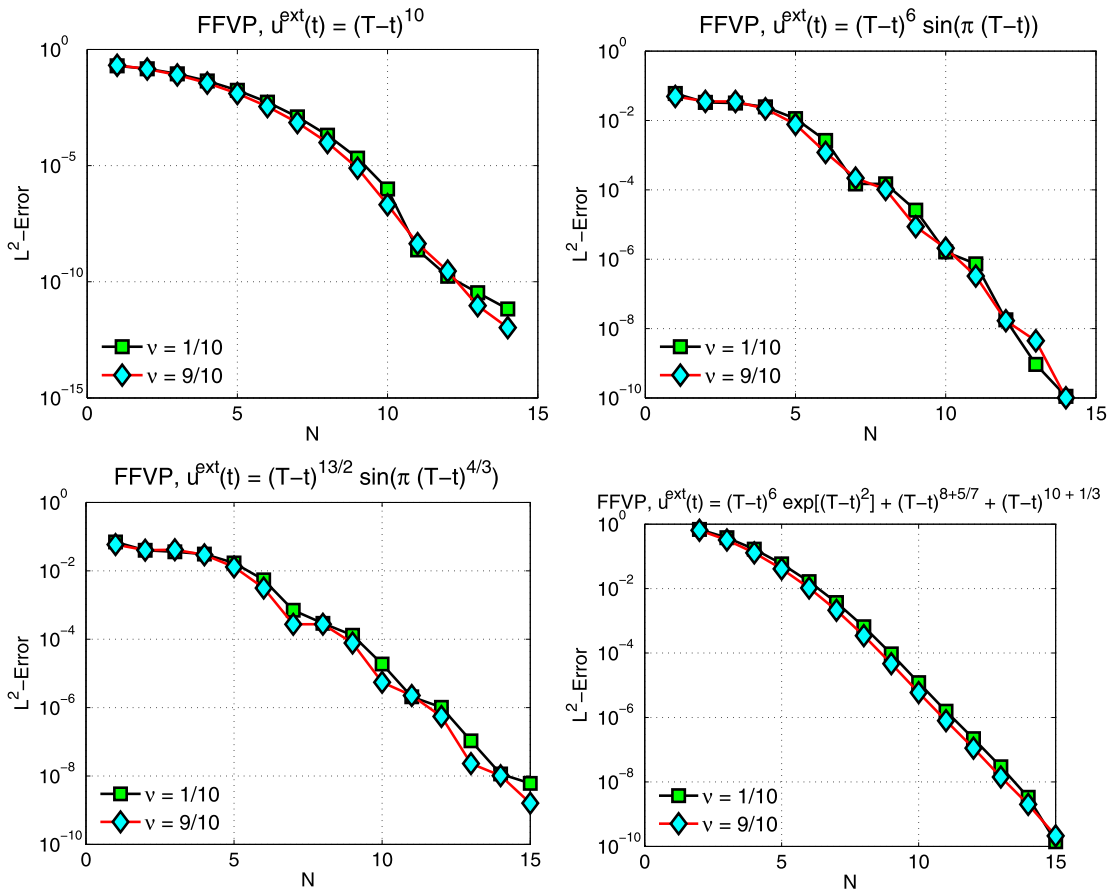


**Fig. 2.** PG spectral method for FFVP: log-linear  $L^2$ -error of the approximate solution to  ${}_t\mathcal{D}_T^\nu u(t) = f(t)$ ,  $t \in [0, 1]$ , versus  $N$ , the order-index in (20), corresponding to  $\nu = 1/10$  and  $9/10$ : (top-left) the exact solution  $u^{\text{ext}}(t) = (T - t)^{10}$ , (top-right) the exact solution  $u^{\text{ext}}(t) = (T - t)^6 \sin(\pi(T - t))$ , (bottom-left) the exact solution  $u^{\text{ext}}(t) = (T - t)^{13/2} \sin(\pi(T - t)^{4/3})$ , and (bottom-right) the exact solution  $u^{\text{ext}}(t) = (T - t)^6 \exp[(T - t)^2] + (T - t)^{8+5/7} + (T - t)^{10+1/3}$ .

exact solutions: (i) monomial  $u^{\text{ext}}(t) = (T - t)^{10}$ , (ii) smooth function  $u^{\text{ext}}(t) = (T - t)^6 \sin(\pi(T - t))$ , (iii) fractional function  $u^{\text{ext}}(t) = (T - t)^{13/2} \sin(\pi(T - t)^{4/3})$ , and finally (iv) combination of fractonomials and a smooth function  $u^{\text{ext}}(t) = (T - t)^6 \exp[(T - t)^2] + (T - t)^{8+5/7} + (T - t)^{10+1/3}$ . In all of these test cases again we obtain exponential convergence.

**4. Discontinuous methods**

In spectral methods developed for FIVP (1) and FFVP (3), the basis functions naturally satisfy the homogeneous initial conditions; however for the case of non-homogeneous initial conditions, we needed to decompose the solution and slightly modify the problem. Next, we present a new *discontinuous spectral element* method to be efficiently employed in *long-time* integration and possible adaptive refinement. To this end, the following lemmas are useful:

**Lemma 4.1.** (See [47].) For  $\mu > 0$ ,  $\alpha > -1$ ,  $\beta > -1$ , and  $\forall x \in [-1, 1]$

$$(1 + x)^{\beta+\mu} \frac{P_n^{\alpha-\mu, \beta+\mu}(x)}{P_n^{\alpha-\mu, \beta+\mu}(-1)} = \frac{\Gamma(\beta + \mu + 1)}{\Gamma(\beta + 1)\Gamma(\mu)P_n^{\alpha, \beta}(-1)} \int_{-1}^x \frac{(1 + s)^\beta P_n^{\alpha, \beta}(s)}{(x - s)^{1-\mu}} ds. \tag{23}$$

By the definition of the left-sided Riemann–Liouville integral and evaluating the special end-values  $P_n^{\alpha-\mu, \beta+\mu}(-1)$  and  $P_n^{\alpha, \beta}(-1)$ , we can re-write (23) as

$${}_{-1}^{\text{RL}}\mathcal{I}_x^\mu \{(1 + x)^\beta P_n^{\alpha, \beta}(x)\} = \frac{\Gamma(n + \beta + 1)}{\Gamma(n + \beta + \mu + 1)} (1 + x)^{\beta+\mu} P_n^{\alpha-\mu, \beta+\mu}(x). \tag{24}$$

Now, by taking the fractional derivative  ${}_{-1}^{\text{RL}}\mathcal{D}_x^\mu$  on both sides of (24) when  $\beta = -\mu$  we obtain

$${}_{-1}^{RL}\mathcal{D}_x^\mu \{P_n^{\alpha-\mu,0}(x)\} = \frac{\Gamma(n+1)}{\Gamma(n-\mu+1)}(1+x)^{-\mu} P_n^{\alpha,-\mu}(x). \tag{25}$$

**Lemma 4.2.** (See [47].) For  $\mu > 0$ ,  $\alpha > -1$ ,  $\beta > -1$ , and  $\forall x \in [-1, 1]$

$$(1-x)^{\alpha+\mu} \frac{P_n^{\alpha+\mu,\beta-\mu}(x)}{P_n^{\alpha+\mu,\beta-\mu}(+1)} = \frac{\Gamma(\alpha+\mu+1)}{\Gamma(\alpha+1)\Gamma(\mu)P_n^{\alpha,\beta}(+1)} \int_x^1 \frac{(1-s)^\alpha P_n^{\alpha,\beta}(s)}{(s-x)^{1-\mu}} ds. \tag{26}$$

By the definition of the right-sided Riemann–Liouville integral and evaluating the special end-values  $P_n^{\alpha-\mu,\beta+\mu}(+1)$  and  $P_n^{\alpha,\beta}(+1)$ , we can re-write (26) as

$${}_{x}^{RL}\mathcal{I}_1^\mu \{(1-x)^\alpha P_n^{\alpha,\beta}(x)\} = \frac{\Gamma(n+\alpha+1)}{\Gamma(n+\alpha+\mu+1)}(1-x)^{\alpha+\mu} P_n^{\alpha+\mu,\beta-\mu}(x). \tag{27}$$

In a similar fashion, by taking the fractional derivative  ${}_{x}^{RL}\mathcal{D}_{-1}^\mu$  on both sides of (27) when  $\alpha = -\mu$  we obtain

$${}_{x}^{RL}\mathcal{D}_{-1}^\mu \{P_n^{0,\beta-\mu}(x)\} = \frac{\Gamma(n+1)}{\Gamma(n-\mu+1)}(1-x)^{-\mu} P_n^{-\mu,\beta}(x). \tag{28}$$

The relations (25) and (28) are useful in computing the corresponding stiffness matrix in the discontinuous scheme presented in the following section.

In the following, we first develop a discontinuous spectral (single-element) scheme for FIVPs (1) and FFVPs (3) and subsequently we extend it to a discontinuous spectral element method in which we partition the computational domain into non-overlapping elements.

#### 4.1. Discontinuous spectral method (DSM; single-element)

We first introduce the spaces of basis and test functions to be employed in the discontinuous scheme for the FIVPs (1). Let  $(-\beta + \mu - 1) \rightarrow 0$  in (7), then  ${}^{(1)}\mathcal{P}_n^{\alpha,\beta,\mu}(x) \rightarrow P_{n-1}^{\alpha-\mu+1,0}(x)$ , where  $\alpha - \mu + 1 = \eta \in (0, 1)$ , since  $-1 \leq \alpha < 2 - \mu$  and  $-1 \leq \beta < \mu - 1$ , recalling from [1]. Hence, in the mapped interval  $[0, T]$ , we define the space of basis functions as

$$\mathcal{V}_N = \text{span}\{\tilde{P}_j^{\eta,0}(x(t)): \eta \in (0, 1), \text{ and } j = 0, 1, \dots, N\}. \tag{29}$$

In a similar fashion, if we let  $(-\alpha + \mu - 1) \rightarrow 0$ , then  ${}^{(2)}\mathcal{P}_n^{\alpha,\beta,\mu}(x) \rightarrow P_{n-1}^{0,\beta-\mu+1}(x)$ , where  $\beta - \mu + 1 = \chi \in (0, 1)$ . In fact in this case  $-1 \leq \beta < 2 - \mu$  and  $-1 \leq \alpha < \mu - 1$ . Hence, we define the space of test functions as

$$\mathcal{V}_N = \text{span}\{\tilde{P}_k^{0,\chi}(x(t)): \chi \in (0, 1), \text{ and } k = 0, 1, \dots, N\}. \tag{30}$$

We call  $\tilde{P}_j^{\eta,0}(x(t))$  and  $\tilde{P}_k^{0,\chi}(x(t))$  asymptotic eigenfunctions of FSLP-I & -II, which are polynomials.

**Remark 4.3.** We shall show how this choice of basis and test polynomial functions leads to efficient and exact calculation of the stiffness matrices arising in the corresponding variational forms using the standard Gauss–Legendre quadrature rules.

##### 4.1.1. FIVP (single-element)

We follow a discontinuous spectral method (DSM) of Petrov–Galerkin kind and seek an approximate solution to (1), where  $u(0) = u_D \neq 0$  generally, in the form

$$u_N(t) = \sum_{n=0}^N c_n \tilde{P}_j^{\eta,0}(x(t)), \tag{31}$$

which  $\forall \vartheta(t) \in \mathcal{V}_N$  satisfies the following variational form obtained from (1) in the time-interval  $I = [0, T]$

$$\left( {}_{0^+}\mathcal{D}_t^{\nu/2} u_N(t), {}_t\mathcal{D}_T^{\nu/2} \vartheta(t) \right)_I - \frac{\vartheta(T)T^{1-\nu}}{(1-\nu)\Gamma(1-\nu)} \llbracket u_N(0) \rrbracket = (f(t), \vartheta(t))_I, \tag{32}$$

where  $(\cdot, \cdot)_I$  denotes the standard inner product in the interval  $I$ , and  $\llbracket u_N(0) \rrbracket = u_N(0^+) - u_N(0^-) = u_N(0^+) - u_D$  represents the jump discontinuity of the solution at the initial condition, and  $\vartheta(T)$  is the test function evaluated at the end of the time-interval. In Appendix A, we provide the derivation of the scheme (32).

We then choose  $\eta = \chi = \nu/2$ , and by substituting (31) into the scheme (32), and taking  $\vartheta(t) = \tilde{P}_k^{0,\chi}(x(t))$  for  $k = 0, 1, \dots, N$ , we obtain

$$\sum_{n=0}^N c_n \left\{ \int_0^T {}_0^+ \mathcal{D}_t^{\nu/2} \tilde{P}_n^{\nu/2,0}(x(t)) {}_t \mathcal{D}_{T^-}^{\eta} \tilde{P}_k^{0,\nu/2}(x(t)) dt - \frac{\tilde{P}_k^{0,\nu/2}(T) T^{1-\nu}}{(1-\nu)\Gamma(1-\nu)} \tilde{P}_n^{\nu/2,0}(0^+) \right\} = \int_0^T f(t) \tilde{P}_k^{0,\nu/2}(x(t)) dt - \frac{\tilde{P}_k^{0,\nu/2}(T) T^{1-\nu}}{(1-\nu)\Gamma(1-\nu)} u_D, \tag{33}$$

where by virtue of (25) and (28) and explicitly evaluating the end points  $\tilde{P}_k^{\nu/2,0}(T^-) \equiv 1$  and  $\tilde{P}_n^{\nu/2,0}(0^+) \equiv (-1)^n$ , (33) yields the following linear system

$$S \vec{c} = \vec{F} \tag{34}$$

where  $S$  denotes the corresponding  $N \times N$  stiffness matrix whose entries are obtained as

$$S[k, n] = \Lambda_{kn} \int_0^T t^{-\nu/2} (T-t)^{-\nu/2} \tilde{P}_n^{\nu,-\nu/2}(x(t)) \tilde{P}_k^{-\nu/2,\nu}(x(t)) dt + \frac{(-1)^{n+1} T^{1-\nu}}{(1-\nu)\Gamma(1-\nu)}, \tag{35}$$

where  $\Lambda_{kn}$  is computed explicitly as

$$\Lambda_{kn} = \frac{\Gamma(k+1)}{\Gamma(k-\nu/2+1)} \frac{\Gamma(n+1)}{\Gamma(n-\nu/2+1)}. \tag{36}$$

In (34), we also compute the load-vector  $\vec{F}$  of size  $N$  as

$$\mathbf{F}[k] = \int_0^T f(t) \tilde{P}_k^{0,\nu/2}(x(t)) dt - \frac{T^{1-\nu}}{(1-\nu)\Gamma(1-\nu)} u_D. \tag{37}$$

**Remark 4.4.** The stiffness matrix  $S$  is a full matrix whose entries satisfy  $S[k, n] = (-1)^{k+n} S[n, k]$ . Hence, we need to compute only half of the entries. Moreover, such entries can be computed *exactly* using the following Gauss quadrature rule thanks to the weight function  $t^{-\nu/2}(T-t)^{-\nu/2}$  arising from the choice of the basis and test functions

$$\int_0^T t^{-\nu/2} (T-t)^{-\nu/2} \tilde{P}_n^{\nu,-\nu/2}(x(t)) \tilde{P}_k^{-\nu/2,\nu}(x(t)) dt \approx \sum_{j=1}^{N+1} \tilde{P}_n^{\nu,-\nu/2}(t_j) \tilde{P}_k^{-\nu/2,\nu}(t_j) \omega_j. \tag{38}$$

This is true since  $\tilde{P}_n^{\nu,-\nu/2} \tilde{P}_k^{-\nu/2,\nu} \in P_{2N}$  for all  $n, k = 1, 2, \dots, N$ . Here,  $t_k$ 's are the Gauss–Lobatto–Jacobi (GLJ) quadrature points in the interval  $[0, T]$  given by

$$t_j = \frac{T}{2} (\xi_j^{-\nu/2, -\nu/2} + 1), \quad j = 1, 2, \dots, N + 1, \tag{39}$$

where  $\xi_j^{-\nu/2, -\nu/2}$  are the standard quadrature GLJ points in  $[-1, 1]$ , and the corresponding weights are obtained as

$$\omega_j = \left(\frac{T}{2}\right)^{1-\nu} \rho_j^{-\nu/2, -\nu/2}, \quad j = 1, 2, \dots, N + 1, \tag{40}$$

in which  $\rho_j^{-\nu/2, -\nu/2}$  represents the standard GLJ quadrature weights associated with the Jacobi parameters  $-\nu/2, -\nu/2$ .

4.1.2. FFVPs (single-element)

We now modify the DSM scheme (32) for solving the FFVPs (3), simply by switching the space of the basis and test functions employed in (32), where this time we employ (30) as our basis space and instead we use (29) as the set of test functions. Then, we seek the approximate solution to (32) where we choose  $u(T) = u_D \neq 0$ , in the form

$$u_N(t) = \sum_{n=0}^N \hat{c}_n \tilde{P}_j^{0,\chi}(x(t)), \tag{41}$$

which  $\forall \vartheta(t) \in V_N$  (set of test functions) satisfies the following variational form

$$({}_t \mathcal{D}_{T^-}^{\nu/2} u_N(t), {}_0^+ \mathcal{D}_t^{\nu/2} \vartheta(t))_I + \frac{\vartheta(0^+) T^{1-\nu}}{(1-\nu)\Gamma(1-\nu)} \llbracket u_N(T) \rrbracket = (f(t), \vartheta(t))_I, \tag{42}$$

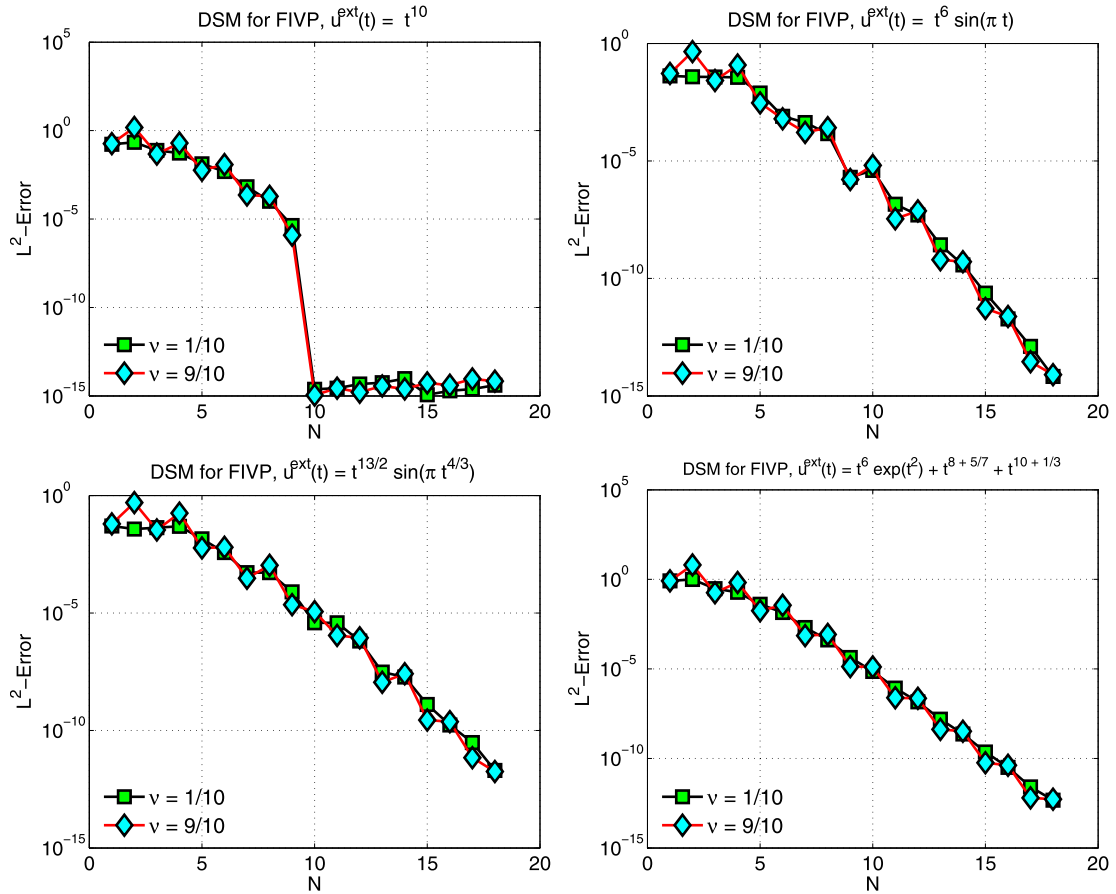


**Fig. 3.** Discontinuous spectral method for FIVP: log-linear  $L^2$ -error of the approximate solution to  ${}_0\mathcal{D}_t^\nu u(t) = f(t)$ ,  $t \in [0, 1]$ , versus  $N$ , the polynomial order in (31), corresponding to  $\nu = 1/10$  and  $9/10$ : (top-left) the exact solution  $u^{\text{ext}}(t) = t^{10}$ , (top-right) the exact solution  $u^{\text{ext}}(t) = t^6 \sin(\pi t)$ , (bottom-left) the exact solution  $u^{\text{ext}}(t) = t^{13/2} \sin(\pi t^{4/3})$ , and (bottom-right) the exact solution  $u^{\text{ext}}(t) = t^6 \exp(t^2) + t^8 + 5/7 + t^{10} + 1/3$ .

where  $[[u_N(T)]] = u_N(T^+) - u_N(T^-) = u_D - u_N(T^-)$  represents the jump discontinuity of the solution at the initial condition, and finally  $\vartheta(0^+)$  is the test function evaluated at the beginning of the time-interval. In Appendix A, we provide the derivation of the scheme (42).

In Figs. 3 and 4, we present numerical results obtained by the DSM scheme to solve the fractional initial-value problem  ${}_0\mathcal{D}_t^\nu u(t) = f(t)$ ,  $t \in [0, 1]$ , and finite-value problem  ${}_t\mathcal{D}_t^\nu u(t) = f(t)$ ,  $t \in [0, 1]$ , corresponding to  $\nu = 1/10$  and  $9/10$ . For the sake of comparison, we consider the same test cases utilized in Figs. 1 and 2. Exponential convergence of both schemes in Figs. 3 and 4 is demonstrated.

4.2. Discontinuous spectral element method (DSEM; multi-element)

Now, we partition the time-interval  $[0, T]$  into  $N_{el}$  non-overlapping time-elements,  $I_e = [t_{e-1/2}, t_{e+1/2}]$  such that  $\bigcup_{e=1}^{N_{el}} I_e = [0, T]$ . Next, we expand the solution in each element  $I_e$  in terms of some basis functions, which are discontinuous at the interfaces of elements and test the problem against another set of test functions space. Here, we construct our basis and test functions based upon (29) and (30), employed in the development of the DPG scheme, as

$$V_h^N = \{v: v|_{I_e} \in V_N(I_e), e = 1, 2, \dots, N_{el}\}, \tag{43}$$

and

$$\mathcal{V}_h^N = \{v: v|_{I_e} \in \mathcal{V}_N(I_e), e = 1, 2, \dots, N_{el}\}. \tag{44}$$

In our discontinuous spectral element method, we seek an approximate solution to (1) on  $e$ -th time-element in the form

$$u_N^e(t) = \sum_{n=1}^N C_n \tilde{P}_j^{\eta,0}(x^e(t)), \tag{45}$$

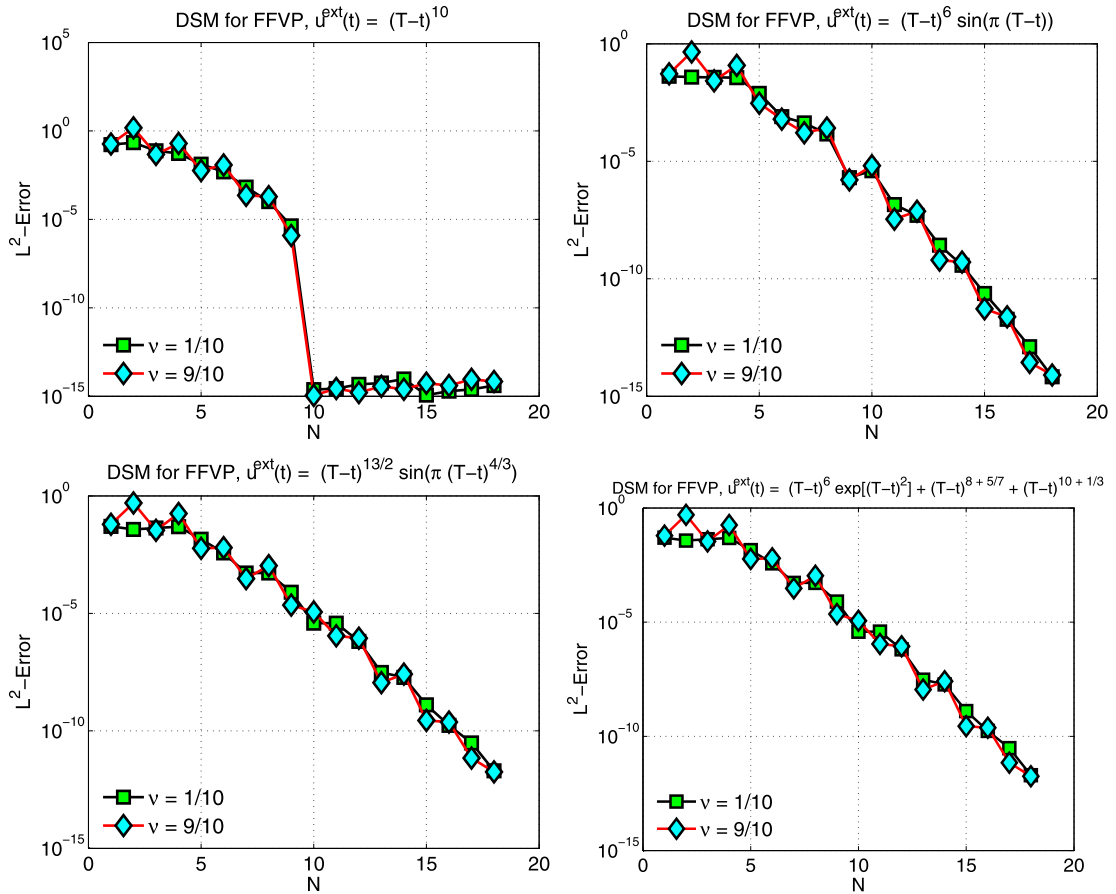


**Fig. 4.** Discontinuous spectral method for FFVP: log-linear  $L^2$ -error of the approximate solution to  ${}_t\mathcal{D}_T^\nu u(t) = f(t)$ ,  $t \in [0, 1]$ , versus  $N$ , the polynomial order in (41), corresponding to  $\nu = 1/10$  and  $9/10$ : (top-left) the exact solution  $u^{\text{ext}}(t) = (T - t)^{10}$ , (top-right) the exact solution  $u^{\text{ext}}(t) = (T - t)^6 \sin(\pi(T - t))$ , (bottom-left) the exact solution  $u^{\text{ext}}(t) = (T - t)^{13/2} \sin(\pi(T - t)^{4/3})$ , and (bottom-right) the exact solution  $u^{\text{ext}}(t) = (T - t)^6 \exp[(T - t)^2] + (T - t)^8 + 5/7 + (T - t)^{10} + 1/3$ .

which  $\forall \vartheta^e(t) \in \mathcal{V}_h^N$  satisfies the following bilinear form originated from projecting (1) onto  $\vartheta^e(t)$  in the time-interval  $I_e = [t_{e-1/2}, t_{e+1/2}]$  as

$$\left( {}_{t_{e-1/2}^+} \mathcal{D}_t^{\nu/2} u_N^e(t), {}_t \mathcal{D}_{t_{e+1/2}^-}^{\nu/2} \vartheta^e(t) \right)_{I_e} - \frac{\vartheta^e(t_{e+1/2}^-) (\Delta t)_e^{1-\nu}}{(1-\nu)\Gamma(1-\nu)} \llbracket u_N^e(t_{e-1/2}) \rrbracket = (f(t), \vartheta(t))_{I_e} - \mathcal{H}_e, \tag{46}$$

beginning from the first element, i.e.,  $e = 1$ , and marching element-by-element along the time-axis to the  $e = N_{el}$ . Here,  $(\Delta t)_e$  emerges the time length of the element  $I_e$ . We note that the only difference between the scheme (46) and the discontinuous spectral (single-element) method in (32) is the *history term*  $\mathcal{H}_e$  appearing on the right-hand side of (46). We shall explain how this term represents an extra *history-load* included in (46). We first write  $\mathcal{H}_e$  in the following convenient and computationally efficient form as

$$\mathcal{H}_e = \vartheta^e(t) F_e(t) \Big|_{t=t_{e-1/2}^+}^{t=t_{e+1/2}^-} - \left( F_e(t), \frac{d}{dt} \vartheta^e(t) \right)_{I_e}, \tag{47}$$

where  $F_e(t)$  is the *history function* associated with element  $I_e$

$$F_e(t) = \sum_{\epsilon=1}^{e-1} \sum_{\delta=0}^N \tau_\delta (t-s)^{\delta+1-\nu} u_N^{(\delta)\epsilon}(s) \Big|_{s=t_{\epsilon-1/2}^+}^{s=t_{\epsilon+1/2}^-} \tag{48}$$

in which  $\tau_\delta = -1/[\Gamma(1-\nu) \prod_{m=0}^{\delta} (m+1-\nu)]$  is decaying with rate  $(\delta-\nu)!$ ,  $\delta = 0, 1, \dots, N$ , and  $u_N^{(\delta)\epsilon}$  represents the  $\delta$ -th derivative of the solution in  $I_\epsilon$  to be only evaluated at the boundaries of  $I_\epsilon$ . We recall that the approximate solution in each element is obtained in terms of the basis functions which are Jacobi polynomials in (29) whose derivatives can be obtained recursively thanks to their hierarchical structure. Hence,  $F_e(t)$  is a *polyfractonomial* of degree  $N + \mu$ , where

$\mu = 1 - \nu \in (0, 1)$ , defined in [1]. Furthermore, we note that when we take  $N_{el} = 1$  in the DSEM scheme, the history-load term  $\mathcal{H}_e = 0$ , then the scheme becomes identical to the DSM scheme (32). In Appendix B, we provide the complete derivation of the scheme (46).

**Remark 4.5.** In order to shed light on the interpretation of such history term in (48) we obtain an alternative representation for the history term (see Appendix B) as

$$\mathcal{H}_e = - \sum_{\epsilon=1}^{e-1} \left( s_\epsilon^0 \mathcal{D}_t^\nu u_N^{\epsilon*}(t), \vartheta^e(t) \right)_{I_e} \Big|_{s_\epsilon^0=t_{\epsilon-1/2}^+}^{s_\epsilon^0=t_{\epsilon+1/2}^-}, \tag{49}$$

where we have continuously extended the solution  $u_N^\epsilon$  from the corresponding element  $I_\epsilon$  to the present element  $I_e$ , denoted by  $u_N^{\epsilon*}$ , such that  $u_N^{\epsilon*}|_{I_\epsilon} = u_N^\epsilon$ . Such a representation implies that the history of the present element  $I_e$  respects the structure of the fractional ODE (1) on the left-hand side. Therefore, assuming any time-continuous extension of the past solution in  $I_\epsilon$  to  $I_e$ , an *extra load* term emerges as a history contribution to the present element.

In order to obtain the corresponding linear system, we choose  $\eta = \chi = \nu/2$ , and by substituting (45) into the scheme (46), and taking  $\vartheta^e(t) = \tilde{P}_k^{0,\chi}(x^e(t))$  for  $k = 0, 1, \dots, N$  and  $e = 1, 2, \dots, N_{el}$ , we obtain

$$\begin{aligned} & \sum_{n=0}^N c_n^e \left\{ \int_{I_e} \mathcal{D}_t^{\nu/2} \tilde{P}_n^{\nu/2,0}(x^e(t)) {}_t\mathcal{D}_{t_{e+1/2}^-}^{\nu/2} \tilde{P}_k^{0,\nu/2}(x^e(t)) dt + (-1)^{n+1} (\Delta t)_e^{1-\nu} \kappa_\nu \right\} \\ &= \int_{I_e} f(t) \tilde{P}_k^{0,\nu/2}(x^e(t)) dt - \kappa_\nu (\Delta t)_e^{1-\nu} (u_N^{e-1})^R - \mathcal{H}_{e,k}, \end{aligned}$$

in which  $\kappa_\nu = 1/[(1 - \nu)\Gamma(1 - \nu)]$ , and hence by Lemma 3.1, we obtain

$$\begin{aligned} & \sum_{n=0}^N c_n^e \left\{ \Lambda_{kn} \int_{I_e} w^e(t) \tilde{P}_n^{\nu,-\nu/2}(x^e(t)) \tilde{P}_k^{-\nu/2,\nu}(x^e(t)) dt + (-1)^{n+1} (\Delta t)_e^{1-\nu} \kappa_\nu \right\} \\ &= \int_{I_e} f(t) \tilde{P}_k^{0,\nu/2}(x^e(t)) dt - \kappa_\nu (\Delta t)_e^{1-\nu} (u_N^{e-1})^R - \mathcal{H}_{e,k}, \end{aligned}$$

where  $w^e(t) = (t - t_{e-1/2})^{-\nu/2} (t_{e+1/2} - t)^{-\nu/2}$  and the term  $(u_N^{e-1})^R$  represents the solution we have already obtained for in element  $I_{e-1}$ , which is evaluated at the right boundary. We note that for  $e = 1$ ,  $(u_N^0)^R$  is equal to the initial condition  $u(0) = u_D$ . The corresponding linear system in element  $I_e$  is then obtained as

$$\mathcal{S}_e \tilde{\mathbf{c}}_e = \tilde{\mathbf{F}}_e \tag{50}$$

where  $\mathcal{S}_e$  denotes the corresponding  $N \times N$  local stiffness matrix in  $I_e$  whose entries are obtained as

$$\mathcal{S}_e[k, n] = \Lambda_{kn} \int_{I_e} w^e(t) \tilde{P}_n^{\nu,-\nu/2}(x^e(t)) \tilde{P}_k^{-\nu/2,\nu}(x^e(t)) dt + (-1)^{n+1} (\Delta t)_e^{1-\nu} \kappa_\nu \tag{51}$$

in which  $\Lambda_{kn}$  is explicitly given in (36). In (50), we also compute the local load-vector  $\tilde{\mathbf{F}}_e$  of size  $N$  as

$$\mathbf{F}_e[k] = \int_{I_e} f(t) \tilde{P}_k^{0,\nu/2}(x^e(t)) dt - \kappa_\nu (\Delta t)_e^{1-\nu} (u_N^{e-1})^R - \mathcal{H}_{e,k}, \tag{52}$$

in which  $\mathcal{H}_{e,k}$  is given by

$$\mathcal{H}_{e,k} = F_e(t_{e+1/2}^-) + (-1)^{k+1} F_e(t_{e-1/2}^+) - \left( F_e(t), \frac{d}{dt} \tilde{P}_k^{0,\nu/2}(x^e(t)) \right)_{I_e}. \tag{53}$$

**Remark 4.6.** Similarly to DSM, the stiffness matrix  $\mathcal{S}_e$  in DSEM scheme is also a full matrix, whose entries similarly follow the property  $\mathcal{S}_e[k, n] = (-1)^{k+n} \mathcal{S}_e[n, k]$ . By the same argument, due to the weight function  $w_e(t)$  appearing as a result of the choice of the basis and test functions the entries of  $\mathcal{S}_e$  can be computed *exactly* using a standard quadrature rule. By performing local element operations and considering an affine mapping from of the physical element to the standard one, we can efficiently compute the entries of  $\mathcal{S}_e$  as

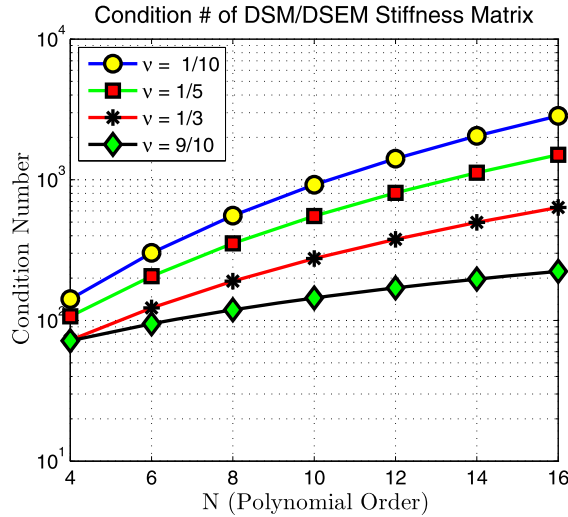


Fig. 5. Condition number of the stiffness matrix obtained in DSM/DSEM in terms of the polynomial order  $N$  and corresponding to different values of the fractional order  $\nu$ . We observe that the condition number grows roughly as  $N^{3-\nu}$ .

$$\begin{aligned}
 S_e[k, n] &= \Lambda_{kn} \int_{I_e} w_e(t) \tilde{P}_n^{\nu, -\nu/2}(x^e(t)) \tilde{P}_k^{-\nu/2, \nu}(x^e(t)) dt \\
 &= J \cdot \Lambda_{kn} \int_{-1}^{+1} (1-x)^{-\nu/2} (1+x)^{-\nu/2} P_n^{\nu, -\nu/2}(x) P_k^{-\nu/2, \nu}(x) dx \\
 &= J \cdot S_e^{st}[k, n],
 \end{aligned} \tag{54}$$

where  $J = [(\Delta t)_e/2]^{1-\nu}$  represents the Jacobian of the transformation and  $S^{st}$  denotes the stiffness matrix on the *standard* element in the interval  $[-1, 1]$ , obtained as

$$S^{st}[k, n] = \Lambda_{kn} \sum_{j=1}^{N+1} P_n^{\nu, -\nu/2}(x_j) P_k^{-\nu/2, \nu}(x_j) \rho_j^{-\nu/2, -\nu/2}, \tag{55}$$

in which  $x_j$ 's are the standard Gauss–Lobatto–Jacobi (GLJ) quadrature points in the interval  $[-1, 1]$  and  $\rho_j$  represent the corresponding weights. The relation (55) shows that in order to compute  $S_e$  in each element, we only need to obtain  $S_e^{st}$  once and multiply it to the corresponding Jacobian in each element. Clearly, on a uniform mesh where  $(\Delta t)_1 = (\Delta t)_2 = \dots = (\Delta t)_{N_{el}} = T/N_{el}$ , the stiffness matrix is invariant in each element and we compute it only *once* for the entire of the simulation.

In addition, we study the condition number of the stiffness matrix in the DSEM and DSM schemes versus the fractional order  $\nu$  and polynomial order  $N$  in Fig. 5. This plot shows that as  $\nu$  decreases the condition number of the stiffness matrix increases. It can be attributed to the fact that the singularity in the definition of the fractional derivative in (1), also the ones appearing in the weight functions  $w(t)$  (DSM) and  $w^e(t)$  (DSEM) become stronger as the fractional order  $\nu$  possesses smaller values. It would suggest that the *global* character of the fractional differential operator in our problem becomes more significant at smaller  $\nu$ , leading to higher stiffness condition numbers. However, we notice in Fig. 5 that as  $\nu \rightarrow 1$ , we recover the standard condition number of the stiffness matrix corresponding to the integer-order (non-fractional) problem.

### 4.3. Numerical tests for DSEM

The  $L^2$ -error of the approximate solution to FIVP  ${}_0\mathcal{D}_t^\nu u(t) = f(t)$ ,  $t \in [0, 1]$ , using discontinuous spectral element method (DSEM), corresponding to  $\nu = 1/2$  is shown in Fig. 6, where the exact solution is  $u^{ext}(t) = t^{10}$ . We compare the log-linear plot of  $p$ -refinement on the left to the  $h$ -refinement, where we observe the exponential convergence in the  $p$ -refinement and the algebraic convergence in the  $h$ -refinement. We show the algebraic convergence rate to be  $-1.673$  in the log-log  $L^2$ -error plot on the right for  $p = 1$  (linear element).

Next, we are going to examine the effect of the fractional order  $\nu \in (0, 1)$  on the order of algebraic convergence, where we require the exact solution to possess enough smoothness. To this end, we present the log-log  $L^2$ -error plot of the approximate solution to FIVP  ${}_0\mathcal{D}_t^\nu u(t) = f(t)$ ,  $t \in [0, 1]$ , obtained using DSEM and corresponding to  $\nu = 1/10$  and  $9/10$

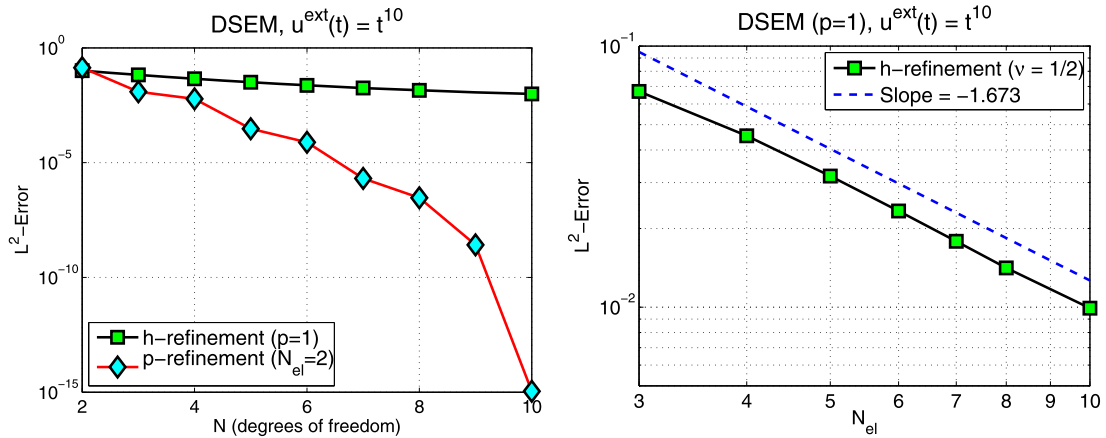


**Fig. 6.** DSEM for FIVP:  $L^2$ -error of the approximate solution to FIVP  ${}_0\mathcal{D}_t^\nu u(t) = f(t)$ ,  $t \in [0, 1]$ , corresponding to  $\nu = 1/2$ ; (left) log-linear plot of  $p$ -refinement compared to the  $h$ -refinement versus the degrees of freedom  $N$ ; and (right) log-log plot of the error versus the number of elements  $N_{el}$ . Here, the exact solution is  $u^{ext}(t) = t^{10}$ .

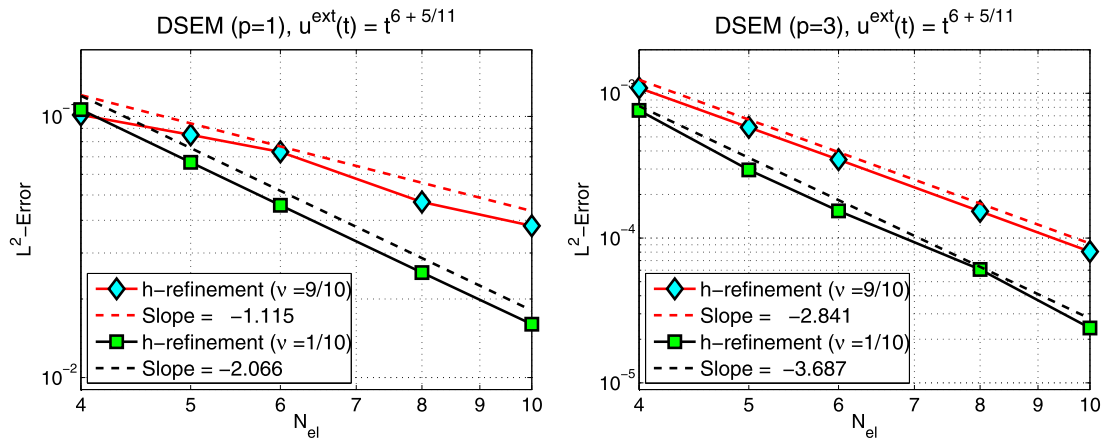


**Fig. 7.** DSEM for FIVP: log-log  $L^2$ -error plot of the approximate solution to FIVP  ${}_0\mathcal{D}_t^\nu u(t) = f(t)$ ,  $t \in [0, 1]$ , corresponding to  $\nu = 1/10$  and  $9/10$  versus the number of elements  $N_{el}$ . Here, the exact solution is  $u^{ext}(t) = t^{6+5/11}$ .

in Fig. 7. The exact solution in this numerical test is  $u^{ext}(t) = t^{2+1/10}$ , and the algebraic order of convergence obtained is  $-1.115$  and  $-2.066$  corresponding to  $\nu = 1/10$  and  $9/10$  respectively, when piecewise linear basis functions are employed. In the other test (Fig. 7; right), we employ piecewise cubic basis functions and we observe the convergence order to be  $-3.687$  and  $-2.841$  corresponding to  $\nu = 9/10$  and  $1/10$  respectively.

In the next test case, we address the issue of the long-time integration. Moreover, we observe that in some cases when the exact solution does not possess enough smoothness  $p$ -refinement may not be the best choice of improving the finite element space  $V_N$ . Accordingly, we take the FIVP  ${}_0\mathcal{D}_t^\nu u(t) = f(t)$ ,  $t \in [0, 10]$ , where  $\nu = 1/2$ , for long-time integration in which the exact solution is  $u^{ext}(t) = t^{1+1/10}$ . The  $L^2$ -error of the approximate solution to the aforementioned problem using DSEM is shown in Fig. 8. The  $h$ -refinement top plot exhibits algebraic convergence with rates  $-1.890$  and  $-1.643$  corresponding to  $\nu = 1/10$  and  $9/10$  respectively. In the middle plot, the log-linear plot of the error versus the number of degrees of freedom  $N$ , compared to the  $p$ -refinements is shown. We observe that the aforementioned  $h$ -refinements are shown to be lower and upper bounds for the decay of the error in the  $p$ -refinements. If we now increase the smoothness in the exact solution as presented in the lower plot, we recover the exponential convergence using  $p$ -refinement where we partition the domain into  $N_{el} = 5$  elements.

Finally, we examine the idea of memory fading/truncation in the calculation of the history term (47). In this technique we do not take all the past elements into account at the expense of losing accuracy, and instead, an effective history length is chosen to calculate (47). Such an effective length is well-known to be dependent mainly on the fractional order  $\nu$ . In fact, the greater  $\nu$  in  ${}_0\mathcal{D}_t^\nu u(t)$  the less history length is needed since as  $\nu \rightarrow 1$ , we approach  ${}_0\mathcal{D}_t^\nu \rightarrow d/dt$ , which is completely a local operator for which no history is required. To this end, we solve  ${}_0\mathcal{D}_t^\nu u(t) = f(t)$ ,  $t \in [0, 1]$ , partitioning the domain into  $N_{el} = 10$  non-overlapping uniform elements when the fractional order is  $\nu = 1/10$ . As shown in Fig. 9, in order to get the convergence down to machine precision, higher modes demand longer history lengths; therefore we need to include

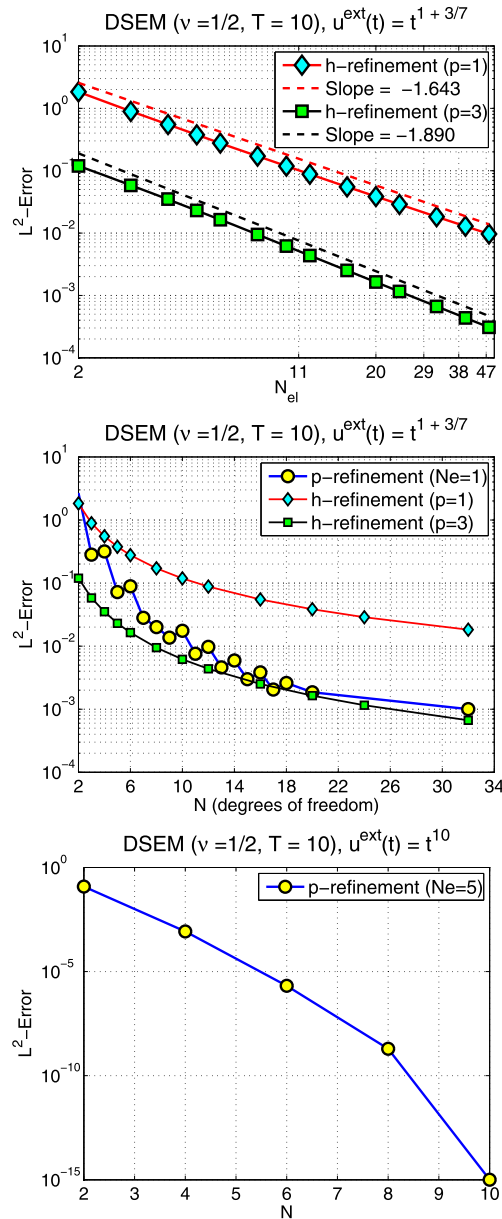


**Fig. 8.** Long-time integration:  $L^2$ -error of the approximate solution to FIVP  ${}_0\mathcal{D}_t^\nu u(t) = f(t), t \in [0, 10]$ , corresponding to  $\nu = 1/2$  obtained using the discontinuous spectral element method (DSEM); (top) log-log plot of the  $h$ -refinement versus the number of elements  $N_{el}$ ; (middle) log-linear plot of the error versus the number of degrees of freedom  $N$ , compared to the  $p$ -refinement; and (bottom) log-linear plot of the error versus the polynomial order in each element in the  $p$ -refinement. Here, the exact solution for the top and the middle plots is  $u^{\text{ext}}(t) = t^{1+3/7}$ , and we add to the regularity of the exact solution in the bottom plot where  $u^{\text{ext}}(t) = t^{10}$ .

the whole history to achieve such an accuracy. We emphasize that such a phenomenon is independent of the discretization method and is solely due to the global nature of the fractional differential operators.

### 5. Summary and discussion

We have developed exponentially accurate spectral methods of Petrov–Galerkin (PG) type for the fractional initial-value problems  ${}_0\mathcal{D}_t^\nu u(t) = f(t)$  and the fractional final-value problem  ${}_t\mathcal{D}_T^\nu u(t) = g(t), \nu \in (0, 1)$ , subject to Dirichlet initial/final conditions. We have employed the recently developed spectral theory in [1] for fractional Sturm–Liouville problems, which provided the corresponding basis and test functions utilized in our schemes. We introduced the corresponding fractional basis functions, called *Jacobi polyfractonomials*, as the eigenfunctions of the FSLP of *first kind* (FSLP-1). Moreover, we employed

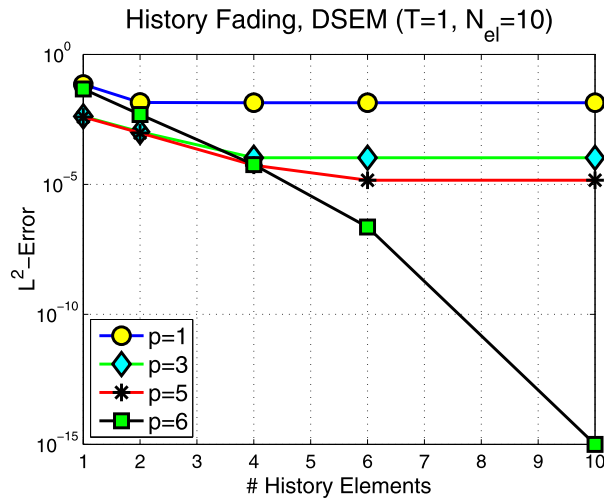


Fig. 9. History fading in DSEM: the  $L^2$ -error of the numerical solution to FIVP  ${}_0\mathcal{D}_t^\nu u(t) = f(t)$ ,  $t \in [0, 1]$ , corresponding to  $\nu = 1/10$  and different polynomial order  $p$ , versus the number of the past elements considered in computation of history function (48). Here, the exact solution is  $u^{ext}(t) = t^6$ .

another space of test functions as the span of polyfractional eigenfunctions of the FSLP of second kind (FSLP-II). In the aforementioned PG spectral methods, the basis functions satisfy the initial/final conditions exactly.

Subsequently, we developed a Petrov–Galerkin discontinuous spectral method (DSM) for the aforementioned FIVPs and FFVPs, and finally extended DSM to a discontinuous spectral element method (DSEM) for carrying out efficient longer time-integrations, but also performing possible discontinuity capturing and adaptive refinement. In both discontinuous schemes, we employed the basis and test functions which were asymptotic eigensolutions to FSLP-I & -II, belonging to the Jacobi family polynomials.

We presented a variety of numerical tests in each case to exhibit the exponential convergence of PG, DSM, and DSEM using  $p$ -refinement; we also investigated the algebraic convergence in DSEM when  $h$ -refinement is performed. In these numerical tests, we considered the exact solution to the FIVPs/FFVPs to be monomials  $t^p$ , smooth functions  $t^q \sin(\pi t)$ , and fractional functions  $t^{p/q} \sin(\pi t^{r/s})$ , where  $p, q, r$  and  $s$  were integers, or any combination of them. In DSEM, we furthermore highlighted the flexibility of the scheme in long-time/adaptive integration.

We have also analyzed the computational complexity of these methods. For example, in Fig. 5 we present the condition number of the stiffness matrix in DSM and DSEM, which seems to grow roughly as  $N^{3-\nu}$ . For the case of PG spectral method, we recall that the stiffness matrix is diagonal due to the orthogonality property of the fractional bases.

We conclude the paper by comparing the performance of the developed schemes with the finite difference method (FDM) developed in [31], where the fractional derivative  ${}_0\mathcal{D}_t^\nu u(t)$  is represented as

$${}_0\mathcal{D}_t^\nu u(t) = \frac{1}{\Gamma(2-\nu)} \sum_{j=0}^k b_j \frac{u(t_{k+1-j}) - u(t_{k-j})}{(\Delta t)^\nu} + r_{\Delta t}^{k+1}, \tag{56}$$

where  $r_{\Delta t}^{k+1} \leq C_u(\Delta t)^{2-\nu}$  and  $b_j := (j+1)^{1-\nu} - j^{1-\nu}$ ,  $j = 0, 1, \dots, k$ ; a central difference method has been employed to approximate the kernel in the fractional derivative.

In Fig. 10, we have solved (1) using DSEM for having the  $T = 10$ ; we plot the normalized  $L^2$ -error versus the number of the elements ( $= T/\Delta t$ ) corresponding to the fractional order  $\nu = 1/10$  and  $\nu = 9/10$ . In DSEM, we utilized both piecewise linear ( $p = 1$ ) and piecewise cubic ( $p = 3$ ) basis functions. First, we observe that when  $\nu = 1/10$ , DSEM ( $p = 1$ ) performs slightly better than FDM in terms of the rate of the convergence in the range of  $h$ -refinement examined (see Fig. 10; left). By increasing the fractional order to  $\nu = 9/10$ , we obtain a good agreement between the rate of convergence in FDM and DSEM ( $p = 1$ ). However, increasing the polynomial order  $p$  (from 1 to 3), DSEM leads to a noticeable faster convergence rate.

In addition to the fast convergence of the high-order methods developed in this work, we show that the computational cost (number of operations) in PG, DSM and DSEM asymptotically increases as  $\mathcal{O}(N)$ ,  $\mathcal{O}(N^3)$ ,  $\mathcal{O}(N_{el}^2 N^3)$ , respectively, where  $N$  represents the polynomial order employed, and  $N_{el}$  denotes the number of elements. In contrast, the computational cost of FDM grows as  $N_g^2$ , where  $N_g$  stands for the number of the grid-points in the computational domain. Moreover, we compute the CPU time (in seconds) required for solving (1) corresponding to  $\nu = 1/10, 1/2$ , and  $9/10$  in Table 1, where the exact solution is  $u^{ext}(t) = t^6$  and the integration time  $T = 1$ . We developed all codes in Wolfram Mathematica 8.0.4.0.

Although the implementation of FDM is simpler than the schemes developed in this study, it turns out that FDM becomes computationally prohibited, especially when we ask for slightly higher accurate results and  $\nu$  is not necessarily close to zero. For instance, in order to reach the  $L^2$ -error of order  $10^{-6}$  using FDM, we needed to include  $N_g = 7500$  grid-points when

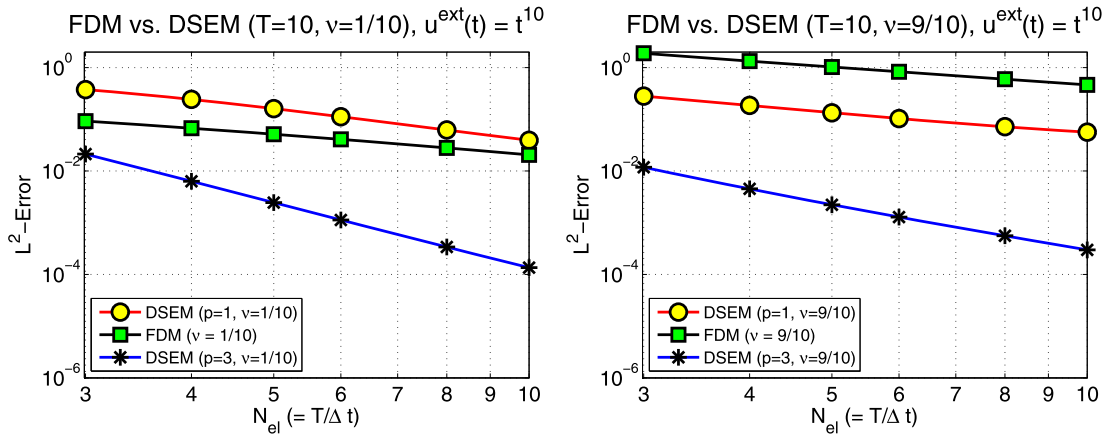


**Fig. 10.** Finite difference method versus discontinuous spectral element method (DSEM);  $L^2$ -norm error (normalized by the  $L^2$ -norm of the exact solution) of the approximate solution to  ${}_0\mathcal{D}_t^\nu u(t) = f(t)$ ,  $T = 10$ , corresponding to (left)  $\nu = 1/10$  and (right)  $\nu = 9/10$ .

**Table 1**

CPU time (seconds) on an Intel (Xeon X5550) 2.67 GHz processor, corresponding to PG spectral method, DSM, DSEM, and FDM for solving  ${}_0\mathcal{D}_t^\nu u(t) = f(t)$ ,  $u(0) = 0$ , and the exact solution is  $u^{ext}(t) = t^6$ . Here,  $N$  denotes the expansion order in PG spectral method, DSM, and DSEM with  $N_{el} = 2$  (in each element), also  $N_g$  represents the number of grid-points in FDM, and the simulation time is set to  $T = 1$ .

$L^2$ -norm error	PG spectral method	DSM	DSEM ( $N_{el} = 2$ )	FDM
$(\nu = 1/10)$				
$\mathcal{O}(10^{-4})$	( $N = 6$ ) 0.0749885	( $N = 5$ ) 0.251108	×	( $N_g = 48$ ) 0.048815
$\mathcal{O}(10^{-5})$	×	×	( $N = 5$ ) 0.390158	( $N_g = 180$ ) 0.24374
$\mathcal{O}(10^{-6})$	( $N = 7$ ) 0.0969855	( $N = 6$ ) 0.344162 (exact)	( $N = 6$ ) 0.652402 (exact)	( $N_g = 640$ ) 3.74287
$(\nu = 1/2)$				
$\mathcal{O}(10^{-4})$	( $N = 6$ ) 0.0584915	( $N = 5$ ) 0.235509	( $N = 4$ ) 0.256461	( $N_g = 340$ ) 0.966354
$\mathcal{O}(10^{-5})$	×	×	( $N = 5$ ) 0.374215	( $N_g = 1600$ ) 23.0223
$\mathcal{O}(10^{-6})$	( $N = 7$ ) 0.073489	( $N = 6$ ) 0.336951 (exact)	( $N = 6$ ) 0.565914 (exact)	( $N_g = 7500$ ) 480.12
$(\nu = 9/10)$				
$\mathcal{O}(10^{-4})$	( $N = 6$ ) 0.076988	( $N = 5$ ) 0.244935	×	( $N_g = 3000$ ) 74.5901
$\mathcal{O}(10^{-5})$	×	×	( $N = 5$ ) 0.389906	( $N_g = 23000$ ) 3348.96
$\mathcal{O}(10^{-6})$	( $N = 7$ ) 0.097985	( $N = 6$ ) 0.343947 (exact)	( $N = 6$ ) 0.645917 (exact)	Running out of memory

$\nu = 1/2$ . By increasing the fractional order to  $\nu = 9/10$ , *Mathematica* ran out of memory and the error level  $10^{-6}$  was not achieved. In fact, it highlights the strong sensitivity of the CPU time in FDM on the fractional order  $\nu$ , in addition to the accuracy dependency of FDM on  $\nu$  as shown in (56). In contrast, the corresponding memory allocation and CPU time in our schemes were considerably less than what needed in FDM. As shown in Table 1, while we exactly capture the solution by just setting the polynomial order to  $N = 6$  in DSM and DSEM in all cases, the CPU time taken in FDM to reach the error level  $10^{-6}$  (when  $\nu = 1/2$ ) was almost 6500 times larger than that in PG spectral method, 1500 times larger than CPU time in DSM, and 850 times larger than that in DSEM. We also performed the CPU time comparison shown in Table 1 for the four test cases shown in Fig. 1, and we obtained similar results.

**Acknowledgements**

This work was supported by the Collaboratory on Mathematics for Mesoscopic Modeling of Materials (CM4) at PNNL funded by the Department of Energy, by OSD/MURI and by NSF/DMS.

**Appendix A. Derivation of the discontinuous spectral method (DSM)**

Let  $I = [0, T]$  be the time-domain and  $\vartheta(t) \in \mathcal{V}_N$  be an arbitrary test function. Then, we obtain a variational form for the solution  $u(t)$  by multiplying (1) by  $\vartheta(t)$  and integrating in  $I$  as

$$({}_0\mathcal{D}_t^\nu u(t), \vartheta(t))_I = (f(t), \vartheta(t))_I. \tag{A.1}$$

On the left-hand side, by the definition of the left-sided fractional derivative we have

$$\begin{aligned}
 ({}_0\mathcal{D}_t^\nu u(t), \vartheta(t))_I &= \int_0^T \frac{1}{\Gamma(1-\nu)} \frac{d}{dt} \int_0^t \frac{u(s) ds}{(t-s)^\nu} \vartheta(t) dt \\
 &= \frac{\vartheta(t)}{\Gamma(1-\nu)} \int_0^t \frac{u(s) ds}{(t-s)^\nu} \Big|_{t=0}^{t=T} - \int_0^T \frac{1}{\Gamma(1-\nu)} \int_0^t \frac{u(s) ds}{(t-s)^\nu} \frac{d}{dt} \vartheta(t) dt \\
 &= \frac{\vartheta(T)}{\Gamma(1-\nu)} \int_0^T \frac{u(s) ds}{(T-s)^\nu} - \int_0^T \frac{1}{\Gamma(1-\nu)} \int_0^t \frac{u(s) ds}{(t-s)^\nu} \frac{d}{dt} \vartheta(t) dt \\
 &= \frac{\vartheta(T)}{\Gamma(1-\nu)} \int_0^{0^+} \frac{u(s) ds}{(T-s)^\nu} + \frac{\vartheta(T)}{\Gamma(1-\nu)} \int_0^T \frac{u(s) ds}{(T-s)^\nu} - \int_0^T \frac{1}{\Gamma(1-\nu)} \int_0^t \frac{u(s) ds}{(t-s)^\nu} \frac{d}{dt} \vartheta(t) dt \tag{A.2}
 \end{aligned}$$

where by carrying out the integration-by-parts in  $\frac{\vartheta(T)}{\Gamma(1-\nu)} \int_0^{0^+} \frac{u(s) ds}{(T-s)^\nu}$  and assuming the exact solution  $u \in C^1[0, T]$  we obtain

$$\frac{\vartheta(T)}{\Gamma(1-\nu)} \int_0^{0^+} \frac{u(s) ds}{(T-s)^\nu} = 0 = \frac{\vartheta(T)T^{1-\nu}}{(1-\nu)\Gamma(1-\nu)} (u_D - u(0^+)) + \frac{\vartheta(T)}{\Gamma(1-\nu)} \int_0^{0^+} (T-s)^{1-\nu} \frac{du(s)}{ds} ds \tag{A.3}$$

where the second integral term in (A.3) is also identically zero. Now, by substituting the exact solution  $u(t)$  by the approximate  $u_N(t)$ , we obtain

$$\frac{\vartheta(T)}{\Gamma(1-\nu)} \int_0^{0^+} \frac{u(s) ds}{(T-s)^\nu} \approx \frac{\vartheta(T)T^{1-\nu}}{(1-\nu)\Gamma(1-\nu)} (u_D - u_N(0^+)) \tag{A.4}$$

where  $(u_D - u_N(0^+)) \neq 0$ , however, as  $N \rightarrow \infty$  this jump discontinuity approaches zero. Now, by substituting (A.4) in (A.2), replacing  $u$  by  $u_N$ , and finally subtracting a zero term  $\frac{\vartheta(0^+)}{\Gamma(1-\nu)} \int_0^{0^+} \frac{u_N(s) ds}{(0^+-s)^\nu}$ , we obtain

$$\begin{aligned}
 ({}_0\mathcal{D}_t^\nu u(t), \vartheta(t))_I &\approx ({}_0\mathcal{D}_t^\nu u_N(t), \vartheta(t))_I \\
 &= \frac{\vartheta(T)T^{1-\nu}}{(1-\nu)\Gamma(1-\nu)} (u_D - u_N(0^+)) + \frac{\vartheta(T)}{\Gamma(1-\nu)} \int_{0^+}^T \frac{u_N(s) ds}{(T-s)^\nu} - \frac{\vartheta(0^+)}{\Gamma(1-\nu)} \int_{0^+}^{0^+} \frac{u_N(s) ds}{(0^+-s)^\nu} \\
 &\quad - \int_0^T \frac{1}{\Gamma(1-\nu)} \int_0^t \frac{u_N(s) ds}{(t-s)^\nu} \frac{d}{dt} \vartheta(t) dt \\
 &= \frac{\vartheta(T^-)T^{1-\nu}}{(1-\nu)\Gamma(1-\nu)} (u_D - u_N(0^+)) + \frac{\vartheta(t)}{\Gamma(1-\nu)} \int_{0^+}^t \frac{u_N(s) ds}{(t-s)^\nu} \Big|_{t=0^+}^{t=T} \\
 &\quad - \int_0^T \frac{1}{\Gamma(1-\nu)} \int_0^t \frac{u_N(s) ds}{(t-s)^\nu} \frac{d}{dt} \vartheta(t) dt \\
 &= ({}_{0^+}\mathcal{D}_t^\nu u_N(t), \vartheta(t))_I + \frac{\vartheta(T^-)T^{1-\nu}}{(1-\nu)\Gamma(1-\nu)} (u_D - u_N(0^+)),
 \end{aligned}$$

where by Lemma 3.1

$$({}_0\mathcal{D}_t^\nu u_N(t), \vartheta(t))_I = ({}_{0^+}\mathcal{D}_t^{\nu/2} u_N(t), {}_t\mathcal{D}_T^{\nu/2} \vartheta(t))_I - \frac{\vartheta(T)T^{1-\nu}}{(1-\nu)\Gamma(1-\nu)} [u_N(0)], \tag{A.5}$$

which completes the derivation of the DSM spectral method for FIVPs by substituting (A.5) into (A.1).

For the derivation of the DSM scheme (42) for FFVPs, we repeat the above steps where this time the jump discontinuity occurs at the final condition. However, we realize that there exists an easier way to do so that is performing the change of variable  $\tilde{t} = T - t$  in (A.5) and Lemma 3.1.

**Appendix B. Derivation of the discontinuous spectral element method (DSEM)**

Now, let  $I_e = [t_{e-1/2}, t_{e+1/2}]$  be the  $e$ -th time-element and  $\vartheta^e(t) \in \mathcal{V}_N$  be an arbitrary test function. Then, we obtain the corresponding variational form by multiplying (1) by  $\vartheta^e(t)$ , and integrating in  $I_e$  as

$$({}_0\mathcal{D}_t^\nu u(t), \vartheta^e(t))_{I_e} = (f(t), \vartheta^e(t))_{I_e}. \tag{B.1}$$

On the left-hand side, by the definition of the left-sided fractional derivative we have

$$\begin{aligned} ({}_0\mathcal{D}_t^\nu u(t), \vartheta^e(t))_{I_e} &= \left( \frac{1}{\Gamma(1-\nu)} \frac{d}{dt} \int_0^t \frac{u(s) ds}{(t-s)^\nu}, \vartheta^e(t) \right)_{I_e} \\ &= \left( \frac{1}{\Gamma(1-\nu)} \frac{d}{dt} \int_0^{t_{e-1/2}^-} \frac{u(s) ds}{(t-s)^\nu}, \vartheta^e(t) \right)_{I_e} \\ &\quad + \left( \frac{1}{\Gamma(1-\nu)} \frac{d}{dt} \int_{t_{e-1/2}^-}^{t_{e-1/2}^+} \frac{u(s) ds}{(t-s)^\nu}, \vartheta^e(t) \right)_{I_e} + \left( \frac{1}{\Gamma(1-\nu)} \frac{d}{dt} \int_{t_{e-1/2}^+}^t \frac{u(s) ds}{(t-s)^\nu}, \vartheta^e(t) \right)_{I_e}, \end{aligned}$$

where by the same argument as in the derivation in Appendix A and also by the definition of the left-sided fractional derivative in the last term we obtain

$$\begin{aligned} ({}_0\mathcal{D}_t^\nu u(t), \vartheta^e(t))_{I_e} &\approx ({}_0\mathcal{D}_t^\nu u_N(t), \vartheta^e(t))_{I_e} \\ &= ({}_{t_{e-1/2}^+} \mathcal{D}_t^\nu u_N^e(t), \vartheta^e(t))_{I_e} + \frac{\vartheta^e(t_{e+1/2}^-)(\Delta t)_e^{1-\nu}}{(1-\nu)\Gamma(1-\nu)} (u_N^{e-1}(t_{e-1/2}^-) - u_N^e(t_{e-1/2}^+)) \\ &\quad + \left( \frac{1}{\Gamma(1-\nu)} \frac{d}{dt} \int_0^{t_{e-1/2}^-} \frac{u(s) ds}{(t-s)^\nu}, \vartheta^e(t) \right)_{I_e} \end{aligned} \tag{B.2}$$

where  $(\Delta t)_e = t_{e+1/2} - t_{e-1/2}$ , and we have replaced  $u$  in the last first and the second term by  $u_N$  and have left the last term unchanged for the following argument. Now, by Lemma 3.1, and the definition of the jump discontinuity we obtain

$$({}_0\mathcal{D}_t^\nu u_N(t), \vartheta^e(t))_{I_e} = ({}_{t_{e-1/2}^+} \mathcal{D}_t^{\nu/2} u_N^e(t), {}_t\mathcal{D}_{t_{e+1/2}^-}^{\nu/2} \vartheta^e(t))_{I_e} - \frac{\vartheta^e(t_{e+1/2}^-)(\Delta t)_e^{1-\nu}}{(1-\nu)\Gamma(1-\nu)} \llbracket u_N^e(t_{e-1/2}) \rrbracket + \mathcal{H}_e. \tag{B.3}$$

We suppose that  $u_N(t)$  is only unknown in the present element  $I_e$  and we have already solved for  $u_N(t)$  in all the previous (past) time-elements. Hence the time-interval  $[0, t_{e-1/2}^-]$ , appearing in the last integral in (B.2), in fact represents a time-history interval. Consequently, we compute  $\mathcal{H}_e$  in (B.3) by decomposing the time-history interval  $[0, t_{e-1/2}^-]$  into the interior past time-elements  $I_\epsilon \equiv [t_{\epsilon-1/2}^+, t_{\epsilon+1/2}^-]$  as

$$\begin{aligned} \mathcal{H}_e &= \left( \frac{1}{\Gamma(1-\nu)} \frac{d}{dt} \int_0^{t_{e-1/2}^-} \frac{u_N(s) ds}{(t-s)^\nu}, \vartheta^e(t) \right)_{I_e} = \sum_{\epsilon=1}^{e-1} \left( \frac{1}{\Gamma(1-\nu)} \frac{d}{dt} \int_{t_{\epsilon-1/2}^-}^{t_{\epsilon+1/2}^+} \frac{u_N^\epsilon(s) ds}{(t-s)^\nu}, \vartheta^e(t) \right)_{I_e} \\ &= \left( \vartheta^e(t) \frac{1}{\Gamma(1-\nu)} \sum_{\epsilon=1}^{e-1} \int_{I_\epsilon} \frac{u_N^\epsilon(s) ds}{(t-s)^\nu} \right) \Big|_{t=t_{e-1/2}^+}^{t=t_{e+1/2}^-} - \left( \frac{1}{\Gamma(1-\nu)} \sum_{\epsilon=1}^{e-1} \int_{I_\epsilon} \frac{u_N^\epsilon(s) ds}{(t-s)^\nu}, \frac{d}{dt} \vartheta^e(t) \right)_{I_e} \end{aligned} \tag{B.4}$$

where  $u_N^\epsilon$  denotes the known solution we have already solved for, and is well-defined only in element  $I_\epsilon = [t_{\epsilon-1/2}^+, t_{\epsilon+1/2}^-]$ . We note that  $u_N^\epsilon$  is a polynomial of degree  $N$ . Therefore,  $u_N^\epsilon$  has  $N$  continuous derivatives in  $I_\epsilon$ . Accordingly, in order to reduce the double integral appearing in the last term in (B.4), we carry out integration-by-parts in  $\int_{I_\epsilon} \frac{u_N^\epsilon(s) ds}{(t-s)^\nu}$   $N$  times to obtain

$$\begin{aligned} \frac{1}{\Gamma(1-\nu)} \sum_{\epsilon=1}^{e-1} \int_{I_\epsilon} \frac{u_N^\epsilon(s) ds}{(t-s)^\nu} &= \sum_{\epsilon=1}^{e-1} \sum_{\delta=0}^N \tau_\delta (t-s)^{\delta+1-\nu} u_N^{(\delta)\epsilon}(s) \Big|_{s=t_{\epsilon-1/2}^+}^{s=t_{\epsilon+1/2}^-} \\ &= \sum_{\epsilon=1}^{e-1} F_e^\epsilon(t) \\ &= F_e(t) \end{aligned} \tag{B.5}$$

where  $F_e(t)$  denotes the flux function associated to the element  $I_e$  in which  $\tau_\delta = \frac{-1}{\Gamma(1-\nu) \prod_{m=0}^\delta (m+1-\nu)}$ . Now, by substituting (B.5) we can efficiently compute the history term as

$$\mathcal{H}_e = \vartheta^e(t) F_e(t) \Big|_{t=t_{e-1/2}^+}^{t=t_{e+1/2}^-} - \left( F_e(t), \frac{d}{dt} \vartheta^e(t) \right)_{I_e} \tag{B.6}$$

where the double integral in (B.4) renders a convenient one-dimensional form in (B.6). It completes the derivation for the fractional discontinuous spectral element scheme given in (46).

Now, we would like to shed more light on the meaning of such history term by re-representing the history term as

$$\begin{aligned} \mathcal{H}_e &= \frac{1}{\Gamma(1-\nu)} \sum_{\epsilon=1}^{e-1} \left\{ \vartheta^e(t_{e+1/2}^-) \int_{t_{\epsilon-1/2}^+}^{t_{\epsilon+1/2}^-} \frac{u_N^\epsilon(s) ds}{(t_{e+1/2}^- - s)^\nu} - \vartheta^e(t_{e-1/2}^+) \int_{t_{\epsilon-1/2}^+}^{t_{\epsilon+1/2}^-} \frac{u_N^\epsilon(s) ds}{(t_{e-1/2}^+ - s)^\nu} \right\} \\ &\quad - \frac{1}{\Gamma(1-\nu)} \sum_{\epsilon=1}^{e-1} \left( \int_{I_\epsilon} \frac{u_N^\epsilon(s) ds}{(t-s)^\nu}, \frac{d}{dt} \vartheta^e(t) \right)_{I_e}. \end{aligned} \tag{B.7}$$

Next, we continuously extend the solution  $u_N^\epsilon$  from the corresponding element  $I_\epsilon$  to the present element  $I_e$ , denoted by  $u_N^{\epsilon*}$ , such that  $u_N^{\epsilon*}|_{I_\epsilon} = u_N^\epsilon$ . In the simplest extension which also sounds natural is to take right-end value of  $u_N^\epsilon$  and consider this constant value in later elements upto  $I_e$ . Having such an extension defined, we can replace  $u_N^\epsilon$  in (B.7) with  $u_N^{\epsilon*}$  and re-write each expression in (B.7) in terms of the subtraction of two integrals as

$$\int_{t_{\epsilon-1/2}^+}^{t_{\epsilon+1/2}^-} \frac{u_N^\epsilon(s) ds}{(t_{e+1/2}^- - s)^\nu} = \int_{t_{\epsilon-1/2}^+}^{t_{\epsilon+1/2}^-} \frac{u_N^{\epsilon*}(s) ds}{(t_{e+1/2}^- - s)^\nu} - \int_{t_{\epsilon+1/2}^-}^{t_{e+1/2}^-} \frac{u_N^{\epsilon*}(s) ds}{(t_{e+1/2}^- - s)^\nu}, \tag{B.8}$$

$$\int_{t_{\epsilon-1/2}^+}^{t_{\epsilon+1/2}^-} \frac{u_N^\epsilon(s) ds}{(t_{e-1/2}^+ - s)^\nu} = \int_{t_{\epsilon-1/2}^+}^{t_{\epsilon+1/2}^-} \frac{u_N^{\epsilon*}(s) ds}{(t_{e-1/2}^+ - s)^\nu} - \int_{t_{\epsilon+1/2}^-}^{t_{e-1/2}^+} \frac{u_N^{\epsilon*}(s) ds}{(t_{e-1/2}^+ - s)^\nu}, \tag{B.9}$$

and

$$\int_{I_e} \frac{u_N^\epsilon(s) ds}{(t-s)^\nu} = \int_{t_{\epsilon-1/2}^+}^t \frac{u_N^{\epsilon*}(s) ds}{(t-s)^\nu} - \int_{t_{\epsilon+1/2}^-}^t \frac{u_N^{\epsilon*}(s) ds}{(t-s)^\nu} \tag{B.10}$$

for any arbitrary  $t \in I_e$ . Now, by substituting (B.8)–(B.10) into (B.7), we obtain

$$\begin{aligned} \mathcal{H}_e &= \sum_{\epsilon=1}^{e-1} \left\{ \frac{\vartheta^e(t)}{\Gamma(1-\nu)} \int_{t_{\epsilon-1/2}^+}^t \frac{u_N^{\epsilon*}(s) ds}{(t-s)^\nu} \Big|_{t=t_{\epsilon-1/2}^+}^{t=t_{\epsilon+1/2}^-} - \frac{1}{\Gamma(1-\nu)} \left( \int_{t_{\epsilon-1/2}^+}^t \frac{u_N^{\epsilon*}(s) ds}{(t-s)^\nu}, \frac{d}{dt} \vartheta^e(t) \right)_{I_e} \right\} \\ &\quad - \sum_{\epsilon=1}^{e-1} \left\{ \frac{\vartheta^e(t)}{\Gamma(1-\nu)} \int_{t_{\epsilon+1/2}^-}^t \frac{u_N^{\epsilon*}(s) ds}{(t-s)^\nu} \Big|_{t=t_{\epsilon-1/2}^+}^{t=t_{\epsilon+1/2}^-} - \frac{1}{\Gamma(1-\nu)} \left( \int_{t_{\epsilon+1/2}^-}^t \frac{u_N^{\epsilon*}(s) ds}{(t-s)^\nu}, \frac{d}{dt} \vartheta^e(t) \right)_{I_e} \right\}, \end{aligned} \tag{B.11}$$

where by inverse integration-by-parts we obtain

$$\mathcal{H}_e = \sum_{\epsilon=1}^{e-1} \left( \frac{1}{\Gamma(1-\nu)} \frac{d}{dt} \int_{t_{\epsilon-1/2}^+}^t \frac{u_N^{\epsilon*}(s) ds}{(t-s)^\nu}, \vartheta^e(t) \right)_{I_e} - \sum_{\epsilon=1}^{e-1} \left( \frac{1}{\Gamma(1-\nu)} \frac{d}{dt} \int_{t_{\epsilon+1/2}^-}^t \frac{u_N^{\epsilon*}(s) ds}{(t-s)^\nu}, \vartheta^e(t) \right)_{I_e} \quad (\text{B.12})$$

and by definition of the left-sided fractional derivative we obtain

$$\mathcal{H}_e = - \sum_{\epsilon=1}^{e-1} \left( {}_{s_\epsilon^0} \mathcal{D}_t^\nu u_N^{\epsilon*}(t), \vartheta^e(t) \right)_{I_e} \Big|_{s_\epsilon^0 = t_{\epsilon-1/2}^+}^{s_\epsilon^0 = t_{\epsilon+1/2}^-}. \quad (\text{B.13})$$

## References

- [1] M. Zayernouri, G.E. Karniadakis, Fractional Sturm–Liouville eigen-problems: Theory and numerical approximations, *J. Comput. Phys.* 47 (3) (2013) 2108–2131.
- [2] M. Ichise, Y. Nagayanagi, T. Kojima, An analog simulation of non-integer order transfer functions for analysis of electrode processes, *J. Electroanal. Chem. Interfacial Electrochem.* 33 (2) (1971) 253–265.
- [3] D.A. Benson, S.W. Wheatcraft, M.M. Meerschaert, Application of a fractional advection–dispersion equation, *Water Resour. Res.* 36 (6) (2000) 1403–1412.
- [4] F. Mainardi, *Fractional Calculus and Waves in Linear Viscoelasticity: An Introduction to Mathematical Models*, Imperial College Press, 2010.
- [5] B.J. West, M. Bologna, P. Grigolini, *Physics of Fractal Operators*, Springer-Verlag, New York, NY, 2003.
- [6] R.L. Magin, *Fractional Calculus in Bioengineering*, Begell House Inc., Redding, CT, 2006.
- [7] J.-P. Bouchaud, A. Georges, Anomalous diffusion in disordered media: statistical mechanisms, models and physical applications, *Phys. Rep.* 195 (4) (1990) 127–293.
- [8] R. Metzler, J. Klafter, The random walk's guide to anomalous diffusion: a fractional dynamics approach, *Phys. Rep.* 339 (1) (2000) 1–77.
- [9] R. Klages, G. Radons, I.M. Sokolov, *Anomalous Transport: Foundations and Applications*, Wiley–VCH, 2008.
- [10] W. Chester, Resonant oscillations in closed tubes, *J. Fluid Mech.* 18 (1) (1964) 44–64.
- [11] J.J. Keller, Propagation of simple non-linear waves in gas filled tubes with friction, *Z. Angew. Math. Phys.* 32 (2) (1981) 170–181.
- [12] N. Sugimoto, T. Kakutani, 'Generalized Burgers' equation' for nonlinear viscoelastic waves, *Wave Motion* 7 (5) (1985) 447–458.
- [13] K. Diethelm, N.J. Ford, Analysis of fractional differential equations, *J. Math. Anal. Appl.* 265 (2) (2002) 229–248.
- [14] A.A. Kilbass, H.M. Srivastava, J.J. Trujillo, *Theory and Applications of Fractional Differential Equations*, Elsevier, Amsterdam, 2006.
- [15] M. Klimek, O.P. Agrawal, On a regular fractional Sturm–Liouville problem with derivatives of order in (0, 1), in: *Proceedings of the 13th International Carpathian Control Conference (ICCC)*, July 2012, 978-1-4577-1868.
- [16] E. Barkai, R. Metzler, J. Klafter, From continuous time random walks to the fractional Fokker–Planck equation, *Phys. Rev. E* 61 (1) (2000) 132.
- [17] N. Sugimoto, Burgers equation with a fractional derivative; hereditary effects on nonlinear acoustic waves, *J. Fluid Mech.* 225 (631–653) (1991) 4.
- [18] B.I. Henry, S.L. Wearne, Fractional reaction–diffusion, *Physica A* 276 (3) (2000) 448–455.
- [19] B. Gustafsson, H.-O. Kreiss, J. Olinger, *Time Dependent Problems and Difference Methods*, vol. 67, Wiley, New York, 1995.
- [20] R.J. LeVeque, *Finite Volume Methods for Hyperbolic Problems*, vol. 31, Cambridge University Press, 2002.
- [21] J.S. Hesthaven, S. Gottlieb, D. Gottlieb, *Spectral Methods for Time-Dependent Problems*, vol. 21, Cambridge University Press, 2007.
- [22] O.C. Zienkiewicz, R.L. Taylor, J.Z. Zhu, *The Finite Element Method: Its Basis and Fundamentals*, Butterworth–Heinemann, 2005.
- [23] G.E. Karniadakis, S.J. Sherwin, *Spectral/hp Element Methods for CFD*, 2nd edition, Oxford University Press, 2005.
- [24] C. Lubich, On the stability of linear multistep methods for Volterra convolution equations, *IMA J. Numer. Anal.* 3 (4) (1983) 439–465.
- [25] C. Lubich, Discretized fractional calculus, *SIAM J. Math. Anal.* 17 (3) (1986) 704–719.
- [26] J. Sanz-Serna, A numerical method for a partial integro-differential equation, *SIAM J. Numer. Anal.* 25 (2) (1988) 319–327.
- [27] R. Gorenflo, F. Mainardi, D. Moretti, P. Paradisi, Time fractional diffusion: a discrete random walk approach, *Nonlinear Dyn.* 29 (1–4) (2002) 129–143.
- [28] K. Diethelm, N.J. Ford, A.D. Freed, Detailed error analysis for a fractional Adams method, *Numer. Algorithms* 36 (1) (2004) 31–52.
- [29] T. Langlands, B. Henry, The accuracy and stability of an implicit solution method for the fractional diffusion equation, *J. Comput. Phys.* 205 (2) (2005) 719–736.
- [30] Z.-z. Sun, X. Wu, A fully discrete difference scheme for a diffusion-wave system, *Appl. Numer. Math.* 56 (2) (2006) 193–209.
- [31] Y. Lin, C. Xu, Finite difference/spectral approximations for the time-fractional diffusion equation, *J. Comput. Phys.* 225 (2) (2007) 1533–1552.
- [32] P. Kumar, O.P. Agrawal, An approximate method for numerical solution of fractional differential equations, *Signal Process.* 86 (10) (2006) 2602–2610.
- [33] J. Huang, Y. Tang, L. Vazquez, Convergence analysis of a block-by-block method for fractional differential equations, *Numer. Math. Theor. Methods Appl.* 5 (2) (2012) 229–241.
- [34] J. Cao, C. Xu, A high order schema for the numerical solution of the fractional ordinary differential equations, *J. Comput. Phys.* 238 (1) (2013) 154–168.
- [35] L. Blank, *Numerical Treatment of Differential Equations of Fractional Order*, Citeseer, 1996.
- [36] E. Rawashdeh, Numerical solution of fractional integro-differential equations by collocation method, *Appl. Math. Comput.* 176 (1) (2006) 1–6.
- [37] M. Khader, On the numerical solutions for the fractional diffusion equation, *Commun. Nonlinear Sci. Numer. Simul.* 16 (6) (2011) 2535–2542.
- [38] M. Khader, A. Hendy, The approximate and exact solutions of the fractional-order delay differential equations using Legendre pseudospectral method, *Int. J. Pure Appl. Math.* 74 (3) (2012) 287–297.
- [39] X. Li, C. Xu, A space–time spectral method for the time fractional diffusion equation, *SIAM J. Numer. Anal.* 47 (3) (2009) 2108–2131.
- [40] X. Li, C. Xu, Existence and uniqueness of the weak solution of the space–time fractional diffusion equation and a spectral method approximation, *Commun. Comput. Phys.* 8 (5) (2010) 1016.
- [41] G. Fix, J.P. Roop, Least squares finite-element solution of a fractional order two-point boundary value problem, *Comput. Math. Appl.* 48 (7) (2004) 1017–1033.
- [42] J.P. Roop, Computational aspects of FEM approximation of fractional advection dispersion equations on bounded domains in  $\mathbb{R}^2$ , *J. Comput. Appl. Math.* 193 (1) (2006) 243–268.
- [43] W. McLean, K. Mustapha, Convergence analysis of a discontinuous Galerkin method for a sub-diffusion equation, *Numer. Algorithms* 52 (1) (2009) 69–88.
- [44] E. Hanert, A comparison of three Eulerian numerical methods for fractional-order transport models, *Environ. Fluid Mech.* 10 (1–2) (2010) 7–20.
- [45] A.R. Carella, *Spectral finite element methods for solving fractional differential equations with applications in anomalous transport*, Ph.D. thesis, Norwegian University of Science and Technology, 2012.
- [46] I. Podlubny, *Fractional Differential Equations*, Academic Press, San Diego, CA, USA, 1999.
- [47] R. Askey, J. Fitch, Integral representations for Jacobi polynomials and some applications, *J. Math. Anal. Appl.* 26 (1969) 411–437.